Synthesis of Polymeric Precursors for Refractory Carbides and Borides

A Thesis

Presented in Partial Fulfillment of the Requirements for the

Degree of Master of Science

with a

Major in Chemical Engineering

in the

College of Graduate Studies

University of Idaho

by

Natalie M. Kirch

Major Professor: Mark Roll, Ph.D.

Committee Members: Krishnan Raja, Ph.D.; Vivek Utgikar, Ph.D.

Department Administrator: D. Eric Aston, Ph.D.

May 2015

Authorization to Submit Thesis

This thesis of Natalie Kirch, submitted for the degree of Master of Science with a Major in Chemical Engineering and titled "Synthesis of Polymeric Precursors for Refractory Carbides and Borides," has been reviewed in final form. Permission, as indicated by the signatures and dates below, is now granted to submit final copies to the college of Graduate Studies for approval.

Major Professor: _____ __Date: _____

Mark Roll, Ph.D.

Committee Members: _____ Date: _____

Krishnan Raja, Ph.D.

_____ Date: _____

Vivek Utgikar, Ph.D.

Department Administrator: _____ __Date: _____

D. Eric Aston, Ph.D.

Abstract

Hafnium Carbide and diboride are ceramics with ultra-high melting temperatures representing the upper end of refractory materials. Current standard syntheses form powders in an energy intensive carbo- (boro-) thermal reduction or coatings via vapor deposition, a time consuming process requiring high vacuum conditions. Research is being done towards an alternative by thermally decomposing preceramic polymers, such as polycarbynes and "polyborynes".

High atomic weight polymer networks enable the conversion from amorphous polymer to ceramic. For synthesis of polycarbynes, studies on Wurtz coupling of sp^3 coordinated bromoform initiated with alkali metals have been published, but these reactions are extremely exothermic and potentially violent.

In an effort to reduce the hazards, reaction set up was performed in a glovebox and the reaction rate was controlled with ultrasonic vibrations. Work towards the "polyboryne" precursor will follow a similar reaction pathway to polycarbyne synthesis.

Acknowledgements

I would like to thank Dr. Mark Roll and the Office of Naval Research for allowing me the opportunity to complete this Master of Science degree.

Also, I would like to recognize Charles Cornwall and Brennett Rodseth in their help of repairing the glove box and building support equipment for my experimental set-up. Brandon Hardie, Jeff Fischer and Isaac Curtis were very accommodating when I needed something plugged in or needed an extra set of hands for plumbing the glove box.

Finally, I am so grateful to Bill Kirch for inspiring two generations of engineers, we miss you Apu.

Table of Contents

List of Figures

List of Tables

List of Equations

Chapter 1 Introduction

Refractory ceramics are stable at high temperatures and retain much of their strength and inertness at those conditions, though they can be very brittle [1, 2]. Carbide, oxide, boride and nitride ceramic families all have refractories that have melting temperatures over 2500°C, as shown in Figure 1. These can be used in a variety of high-temperature applications like furnace elements, thermal protection systems, and plasma arc electrodes [3, 4].

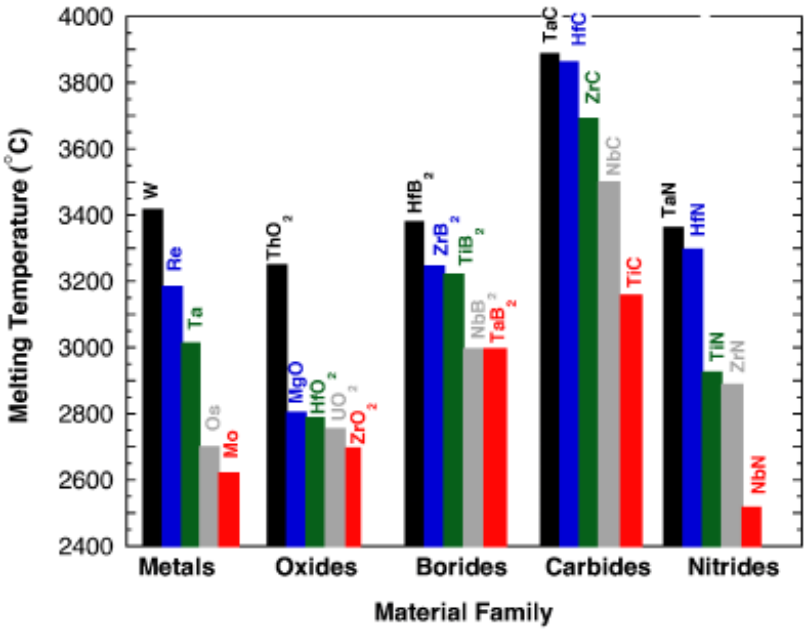

Figure 1 Melting Temperatures of the Most Refractory Members of Select Material Families [5]

Hafnium Carbide and diboride are ultra-high temperature ceramics (UTHC) representing the upper end of refractory materials, known for their heat resistant properties. Hafnium diboride has a melting point at approximately 3250°C [6] and high thermal conductivity [7]. Hafnium carbide has a melting point of 3900°C and also exhibits high thermal and electrical conductivity [8, 9]. Metals in Group 4, the same group as hafnium, like titanium and zirconium, exhibit similar properties and can be used as analogs in reactions.

Though Group 4 carbides and diborides have attractive chemical properties, their mechanical properties are greatly limited by mechanical and physical properties affected by the densification process, starting powders and the difficult sinterability [10]. Current standard synthesis of UTHC form either powders [3, 5]in heat intensive carbo- or boro-thermal reduction or coatings via vapor deposition [11] which is time consuming and requires high vacuum conditions. Additionally these methods are limited the geometries they can be applied [6]. An alternative is thermally decomposing the polymer preceramics, polycarbynes and "polyborynes," into the ceramic film.

"Chimie douce" methods are part of a trend to control the synthesis and properties of material [12]. A polymer solution can be spun, molded or cast to form films and uniform coatings. A high molecular weight bonding network rather than two dimensional chains, converts from amorphous to ceramic structure upon application of heat [11]. The first polymer preceramics formed silicon carbide fibers from polycarbosilanes through pyrolysis [13]. With Wurtz coupling or hydrosilylation, organosilanes bisubstituted with halides, were coupled into polycarbosilanes [13, 14]. During pyrolysis, crosslinking occurs binding the chains together, though crystallization doesn't start occurring until 1100°C when β-SiC formation begins [13]. Better yields occur when crosslinking is included in the polymer structure [12].

Application as Thermal Protection Systems

The resistance to corrosion and wear, even at high temperatures, make Group 4 carbides and diborides specifically ideal for thermal protection systems [15]. These are important for hypersonic applications, like the leading edge of reusable re-entry aerospace vehicles, where surface temperatures are expected at least to 2400°C [4, 15]. A sharp leading edge is effectively an edge radius that is much smaller than the object's length scale, which can reduce the object's drag [7]. However, the smaller the radius, the higher the convective heating is which increases the surface temperature [7]. Figure 2 shows the heat profile on a leading edge. Oxidation from air flow is a limiting factor of application, as the oxide layer can have a reduced melting temperature [5, 9].

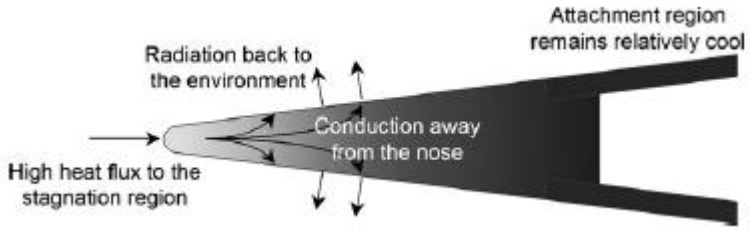

Figure 2 Leading Edge Thermal Management [7]

Current thermal and oxidation barrier coatings are typically silicon based ceramics, like silicon carbide [10]. The silicon ceramics form a protective SiO_2 layer that is stable up to 1600°C [10]. An approach to incorporate Group 4 carbides and diborides uses carbide and silicon carbide fibers as reinforcement, unfortunately the useable temperature limit is still 1600°C due to oxidation of the fibers [10]. Ideally uniform UHTCs can be developed to replace these composites.

Oxidation Resistance

The HfO_2 and ZrO_2 that forms through oxidation are refractory materials, as seen in Figure 1, and HfO_2 is stable up to 2200°C and forms a protective layer on the non-oxide surface [16]. This oxide barrier effectively creates a multilayer coating, preventing oxygen diffusion that may otherwise occur on the substrate without the carbide or diboride [17]. The binary phase diagram of hafnium and oxygen, focused on the HfO_2-rich portion is shown in Figure 3.

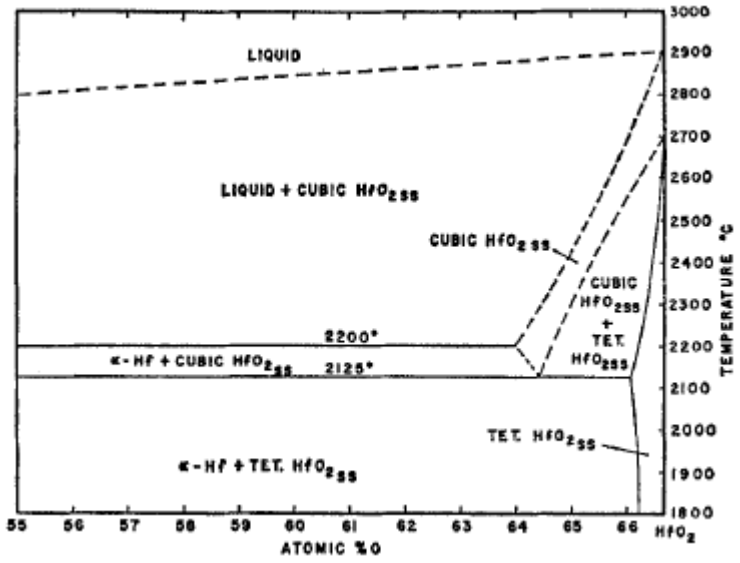

Figure 3 Hafnia-rich Hf-O Binary Phase Diagram [18]

Carbides of Group 4 metals have lower oxidation resistance when compared to their respective diborides [4], with an upper limit of 1100-1400°C for hafnium carbide [2]. Hafnium and zirconium oxides stability increases the carbides' resistance to ablation [19]. Studies of ablation effects on HfC found that a uniform tetragonal HfO_2 layer forms on the hafnium carbide surface after ablation at 3000°C for 240s, protecting the hafnium carbide from further oxidation [19]. Though the hafnium carbide reacts with its oxide, the reaction reaches equilibrium when the partial pressure of carbon monoxide reaches 0.01mmHg (13.3Pa) [17].

Research in oxidation resistance, accumulated by Opeka et al., for diborides at temperatures between 1200-2200°C revealed that Group 4 diborides were resistant to oxidation, with hafnium having the greatest resistance [4]. Additionally refractory diborides are relatively stable in the presence of moisture [2]. Metal rich diborides like $HfB_{1.7}$ have greater oxidation resistance than boron rich diborides like $HfB_{2.12}$; and presence of water vapor in the $He\text{-}O_2$ test gas increased the rate of oxidation by a factor of five in these non-stoichiometric ceramics [4].

Carbides

Pyrolytic carbide films, like the kind synthesized by Bianconi et al., have been deposited as polycrystalline continuous films, as shown in Figure 4. When Bianconi et al. sputtered gold on the surface of the film; the apparent topography disappeared, meaning that the features are different regions of crystallinity, density or degree of electron charging, rather than variations in film thickness [11]. These films have not been duplicated with the inclusion of Group 4 metals.

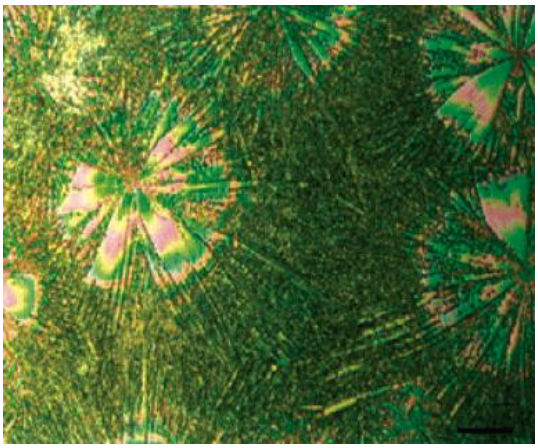

Figure 4 Diamond-like carbon film from poly(hydridocarbyne) on a silicon substrate, scale bar = 50 microns [11]

UV Raman spectra of the diamond-like film does not resemble the typical diamond cubic crystal structure [11]. Instead it is closer to the Wurtzite hexagonal polymorph, unrelated to the Wurtz coupling, known as Lonsdaleite [20], which has only been seen in synthetic diamonds and at the site of meteor impacts [21]. Figure 5 shows the comparison of the spectra. Figure 6 and Figure 7 show the difference between the cubic and hexagonal structures.

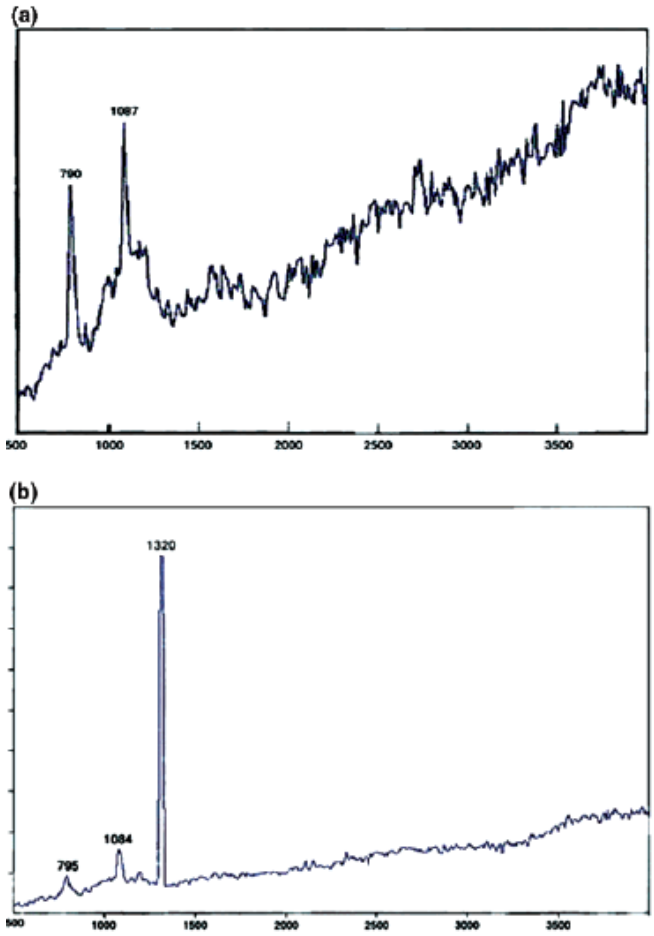

Figure 5 (a) UV Raman (244 nm) of a diamond-like carbon film on a silicon substrate, (b) UV Raman (244 nm) of hexagonal diamond [11]

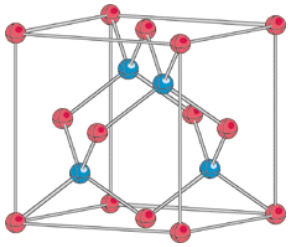

Figure 6 Diamond cubic structure (red on the face) [22]

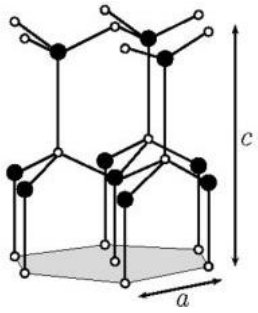

Figure 7 Lonsdaleite (Diamond-Wurtzite) Hexagonal Structure [23]

Group 4 Carbides

Carbides may be divided into three types: ionic, covalent and interstitial [2]. Ionic carbides contain cations from Group 1, 2 or 3; only two refractory covalent carbides have been observed, SiC and B_4C; and hafnium carbide falls within the third category of interstitial metal carbides, which contains most carbides of Group 4, 5 and 6 [2]. Typically hafnium carbide exhibits rock salt-like cubic closed packed bonding of HfC, but is also expected to be stable as Hf_3C_2 and Hf_6C_5, both of which would bond in a monoclinic C2/m structure [24]. Figure 8 shows the crystal structure of HfC, which has a lattice constant, *a*, between 4.609Å and 4.639Å [24].

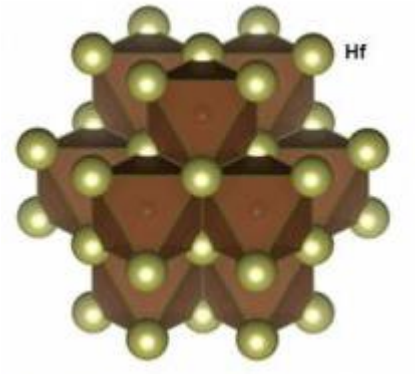

Figure 8 Crystal Structure of HfC [24]

Opeka et al.conducted a comparison of the thermal and mechanical properties of HfB_2, $HfC_{0.98}$, $HfC_{0.67}$ and $HfN_{0.92}$ [3]. They measured the lattice parameters for $HfC_{0.98}$ and $HfC_{0.67}$ to be 4.6433Å and 4.6237Å respectively [3]. Thermal conductivity increases with increasing carbon, but less than that of the diboride, data collected by Opeka et al.is shown in Figure 9. The thermal conductivity of $HfC_{0.98}$ was twice that of $HfC_{0.67}$ [3].

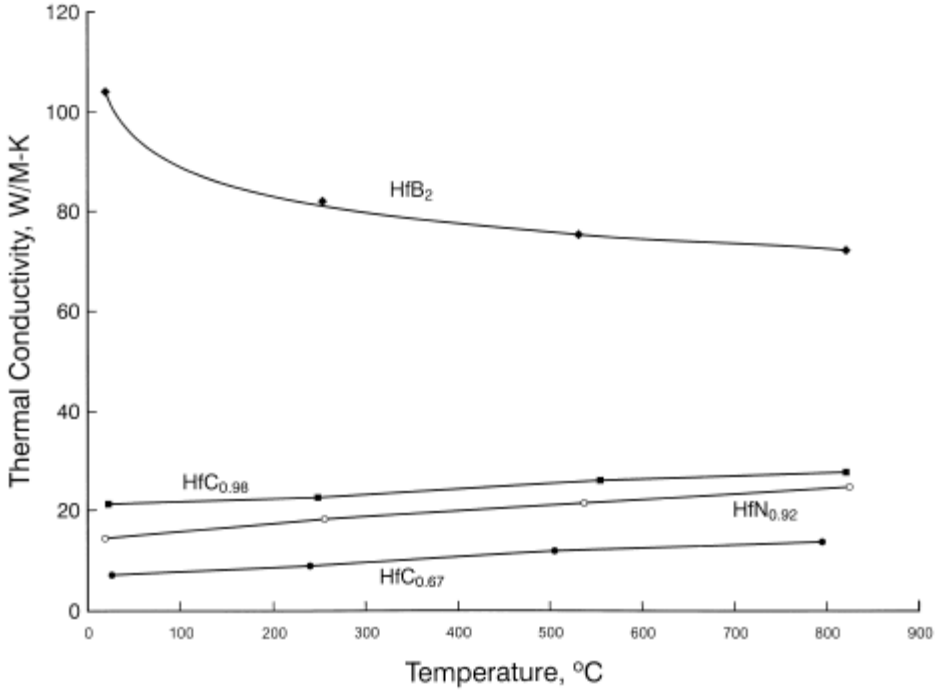

Figure 9 Thermal Conductivity of HfB_2, $HfN_{0.92}$, $HfC_{0.67}$, $HfC_{0.98}$ [3]

Diborides

Metal boride ceramics can bond within a range of compositions and the ratio of boron to metal in the material effects the electron behavior and bonding structure [5]. Boron can form diboride compounds within Groups III-VI and Periods 4-6 (Groups 3-7 and 13-16 in the IUPAC convention) within the Periodic Table. As the atomic number increases, the hardness of the metal diboride decreases [5]. Figure 10 shows the cage-like hexagonal structure of aluminum diboride.

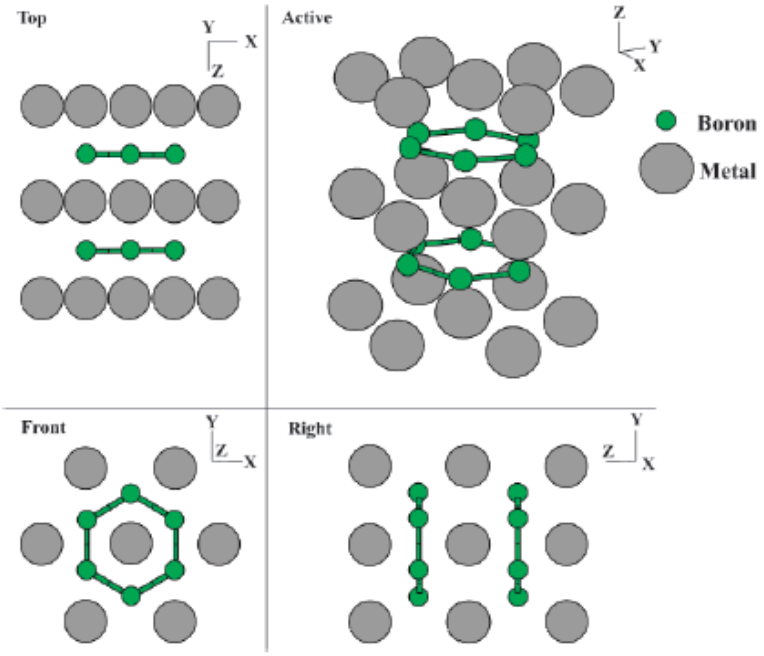

Figure 10 Projections of the Diboride Structure [5]

Metal diborides tend to form sp^2 and sp^3 hybrid orbitals, although it will often be in a combination of the two [5]. This lowers their hardness and brittleness compared to their corresponding carbides, as a typical carbide ceramic only exhibits sp^3 hybridization.

Diboride preceramics have yet to be coated as pure polymer and instead have been used for binding ceramic powders or as chemical vapor (CVD) deposition sources [5]. Fujii and Ozawa did form a viscous liquid of $Mg(BH_4)_2$, as shown in Equation 10, but ground down their pyrolyzed ceramic for analysis [25]. As powders, the transition to ceramic crystals has only yielded micrometer and nanometer sized individual crystalline domains shown in the work done by Fahrenholtz et al [5] , and by Fujii and Ozawa [25]. Segal has identified soluble polymer preceramics in his work with boron nitride systems as an alternative if the polymer is too difficult to coat as a powder [26].

Hoekstra and Katz note that boron hydrides are volatile, with the boron hydrides of aluminum, beryllium and uranium (IV) are the most volatile compound of each metal [27]. Their experiments found that the melting points of hafnium borohydride and zirconium borohydride to be 29.0°C and 28.7°C respectively [27]. The vapor pressures of hafnium and zirconium borohydride are in Table 1. Hoekstra and Katz found that the volatile Group IV-B (Group 4) borohydrides would decompose at room temperature to release hydrogen and presumably leave the metal boride behind [27].

VAPOR PRESSURES OF THORIUM, HAFNIUM AND ZIRCONIUM BOROHYDRIDES (MM.)

Compound → Temp., °C.	Thorium borohydride	Hafnium borohydride	Zirconium borohydride
0		2.2	1.8
10		4.7	4.2
25		14.9	15.0
30		21.0	20.3
40		36.0	33.2
50		56.4	52.2
130	0.05		
150	.20		

Table 1 Vapor Pressures of Thorium, Hafnium and Zirconium Borohydrides in mmHg [27]

Wayda et al.took these findings by Hoekstra and Katz and used them for low-temperature deposition, confirming the composition of the degradation product as diboride [28]. Their vapor phase transport of zirconium and hafnium diborides occurred at 0°C [28]. The thermal decomposition to the metal diboride was achieved with a set point of 196°C, and due to temperature variance in their tube furnace, transition to ceramic diboride occurred on the portions above 100°C [28].

Boron Hydride Cluster Conversion to Diborides

Magnesium borohydride has been thermally decomposed to magnesium diboride at temperatures as low as 300°C [29]. This process is reversible via heated ball milling, which reintroduces hydrogen into the system and forms the dodecaborohydride as a side product. However, this study by Gupta et al.did not focus on the dodecaborohydride and instead focused on magnesium borohydride to diboride conversion [29]. The reaction pathways during reactive ball milling are shown in Equation 1, Equation 2, Equation 3 and Equation 4.

$$Mg(BH_4)_2 \rightarrow MgB_2 + 4H_2$$

Equation 1 Dehydrogenation of Magnesium Borohydride at 300°C [29]

$$Mg(BH_4)_2 \rightarrow {}^{1}/_{6}\,MgB_{12}H_{12} + {}^{5}/_{6}\,MgH_2 + {}^{13}/_{6}\,H_2$$

Equation 2 Side Reaction of Magnesium Borohydride Dehydrogenation Between 280°C and 350°C [29]

$$MgB_{12}H_{12} \rightarrow Mg(or\ MgH_2) + 12B + 6H_2(or\ 5H_2)$$

Equation 3 Side Reaction of Magnesium Borohydride Dehydrogenation at 355°C [29]

$$MgH_2 \rightarrow Mg + H_2$$

Equation 4 Dehydrogenation of Magnesium Hydride at 410°C [29]

Goedde and Girolami have done a preliminary study of attaching chromium to octahydrotriborate as a CVD precursor to metal diborides [30]. The structure is shown in Figure 11; note that it is symmetrical. The complex with chromium is liquid and thermally unstable, and the vapor deposition of CrB_2 could occur when heated above 200°C [30].

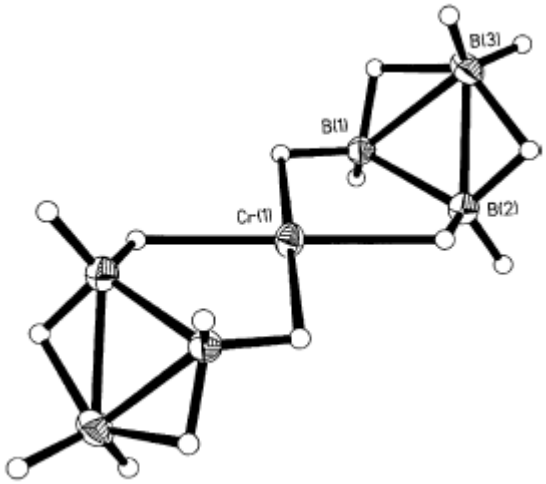

Figure 11 Molecular Structure of $Cr(B_3H_8)_2$ [30]

Carbon Preceramic

Wurtz Coupling

Initially in forming the carbide, to guarantee a highly networked carbon based polymer, sp^3 bonding must be maintained. Wurtz coupling is when the central group of a molecule, like the organic backbone of an organohalide bonds to the organic group from the same species, initiated by an active metal like sodium or lithium, forming an organic pair and two salt molecules [31]. With additional halides attached to the base structure there are more orientations for the coupling, as well as initiating polymerization [32].

Bianconi et al [11, 33] have been working on synthesizing diamond-like carbide films following a similar pathway as the silicon carbide formation: Wurtz coupling to form the preceramic, thermally driving off the excess hydrogen and completing the lattice structure by crosslinking. A tri-substituted alkyl halide like bromoform or chloroform is used to drive sp^3 coupling [11]. Equation 5 shows the synthesis reaction for poly(hydridocarbyne), a structural isomer of polyacetylene, by coupling bromoform to itself with an alloy of sodium and potassium as the active metal.

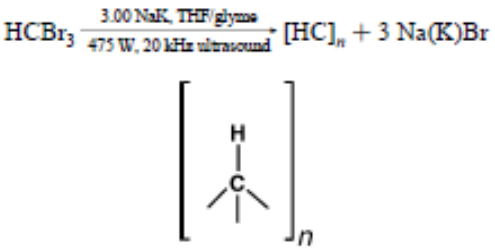

Equation 5 Wurtz Coupling of Bromoform [11]

Wurtz coupling has also been applied to polymers with tin backbones [32], in addition to carbon and silicon backbones, showing the versatility of the mechanism. Previous work by Visscher and Bianconi [33] followed synthesis methods of network copolymer polysilynes with Group 4 metals to prepare analogous networks with poly(phenylcarbyne), shown in Equation 6, where R is cyclopentane (Cp) or the radical of cyclopentane (Cp*), and M is either titanium or hafnium, respectively.

$$0.75PhCCl_3 + 0.25RMCl_3 \xrightarrow{3NaK,THF\ (475W,20kHz\ ultrasound)} [(PhC)_x(RM)_{1-x}]_n$$

Equation 6 Metal incorporated block copolymer synthesis [33]

The coreduction of 75% $PhCCl_3$ with 25% $CpTiCl_3$ with titanium forms a polymer with the empirical formula of $[(PhC)_{0.98}(CpTi)_{0.02}]_n$, which mostly yielded soluble oligomeric material though there was the presence of cross-linked material [33]. Low yields could be due to the bulky nature of the cyclopentyl-titanium groups. The corresponding hafnium coreduction forms a polymer with the empirical formula of $[(PhC)_{0.95}(Cp^*Hf)_{0.05}]_n$, which only manifested as soluble oligomers. However the hafnium oligomers were of higher molecular weights than the titanium oligomers [33].

Key to the reaction rate of Wurtz coupling is the surface area of the sodium, or other active metal. In the past, this has meant raising the reaction temperature to 98°C, the melting temperature of sodium [14]. Unfortunately due to the high reactivity of sodium, especially with an alkyl halide, Wurtz coupling is often violently exothermic as well as oxygen sensitive [32, 34]. Work on creating emulsions via sonication or complexes with the activated metals have added a degree of safety and control [14, 34].

Sonication

Sodium dispersions in organic mediums like petroleum jelly or ammonia have both the advantage of high surface area for reactions and are protected from air and water vapor [35]. A comparison of reaction of sodium and monochlorobenzene, an exothermic reaction with both mechanically and ultrasonically dispersed sodium. The sodium is dispersed in light petroleum (boiling point between 100-120°C) and the change in reaction rate is shown in Figure 12 [35]. In the mechanically dispersed sample the temperature increases slowly at first and then exponentially increases to an unstable point, but then rapidly drops off before completion. The ultrasonically dispersed sample has a high initial reaction rate that quickly tapers to a steady state temperature and levels off at completion.

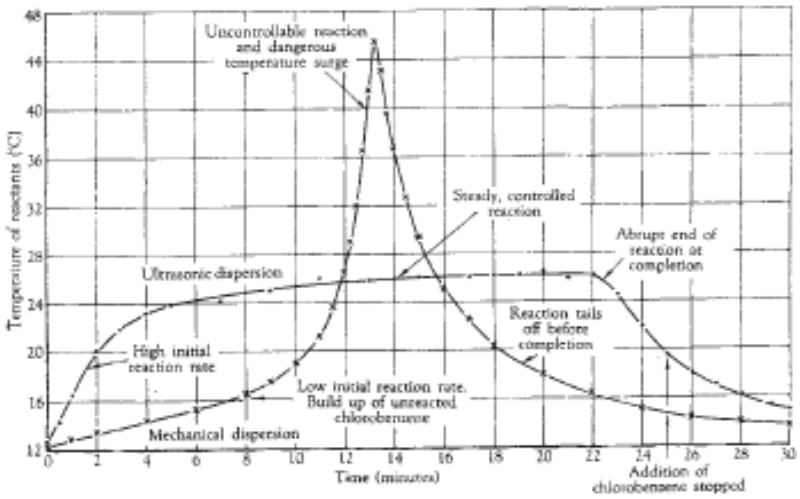

Figure 12 Reactivity comparison of sodium dispersed mechanically and ultrasonically [35]

Miller et al.studied the effects sonication of Wurtz coupling on the polymerization of substituted dichlorosilanes, though sonication did not uniformly have better yield for all of their structurally different monomers, it did allow for room temperature reactions [14]. Bianconi et al. also used sonication to initiate Wurtz coupling to better control the reaction rate [11]. In a liquid, intermolecular forces create cohesion that manifests itself macroscopically as properties such as surface tension, viscosity and volatility [36]. Cohesion is affected by gas bubbles and solid particles present in the liquid. Ultrasonic vibrations can create unstable gas or vapor bubbles that can compress and collapse into instantaneous conditions of high temperature and pressure [35, 36].

Oligomerization

When synthesizing a polymer, there is an upper limit to the power input from the ultrasound. There needs to be a balance between a well dispersed emulsion for polymerization and shearing from the vibrations [11]. The newly formed oligomers allow for increased sp^2 bond formation when the nearest available carbons to fill the newly opened bond are already bonded to each other; and it disrupts the transition to ceramic by creating amorphous zones.

Pyrolysis

Pyrolysis, the thermal decomposition of a substance in an inert environment, drives off the excess hydrogen in the preceramic converting it to a crystalline or polycrystalline substance. Conversion properties, decomposition temperature for instance, are dependent on the processing conditions, like the polymer molecular weight, the state of the polymer (e.g. powder or film), and ramp rate of the pyrolysis furnace [11]. A highly networked polymer will mimic the lattice of the ceramic, and when the hydrogen is removed the new bonding pairs will finish building the lattice.

Pyrolysis work towards silicon carbide fibers found that the Si-Si bonds cleave before the Si-C, Si-H and C-H due to the bond energy being the lowest [37]. The Si-C bonds are more resistant than the C-H bonds to the free radical that forms upon the Si-Si bond cleavage, and dehydrogenation allows for the polymerization to continue [37]. The reaction mechanism is shown in Equation 7 and the polymer structure is shown in Figure 13.

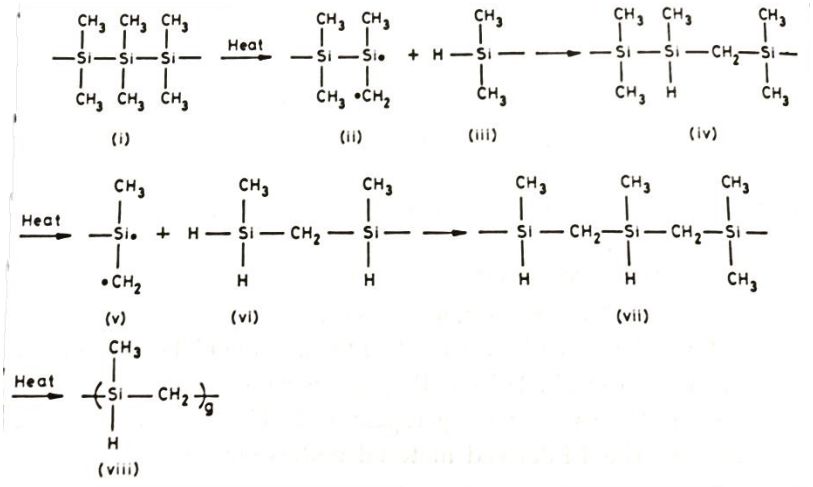

Equation 7 Crystallization to β-SiC [37]

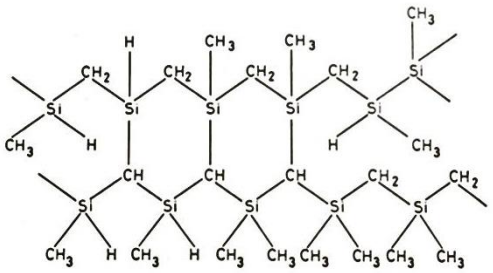

Figure 13 Polycarbosilane Structure [37]

Diboride Preceramic

Borohydride Decomposition

Amorphous metal borohydrides or –carbides can be used in an analogous process to the polycarbyne synthesis as they decompose into diborides [6, 25]. Fahrenholtz et al.synthesized nanocrystalline hafnium diboride via anhydrous hafnium chloride and sodium borohydride at above 500°C and under pressure, shown in Equation 8 [5]. In the vapor phase the sodium borohydride decomposes to borane before reacting with the gaseous chloride. The resulting hafnium diboride crystals were in the range of 10-20 nm [5].

$$HfCl_{4(g)} + 2NaBH_{4(g)} \rightarrow HfB_{2(c)} + 2NaCl_{(c)} + 2HCl_{(g)} + 3H_{2(g)}$$

Equation 8 Synthesis of Hafnium Diboride [5]

They also thermally decomposed titanium borohydride into titanium diboride shown in Equation 9. The crystals in this reaction were 100-200 nm in diameter [5].

$$2Ti(BH_4)_{3(c)} \rightarrow 2TiB_{2(c)} + B_2H_{6(g)} + 9H_{2(g)}$$

Equation 9 Synthesis of Titanium Diboride [5]

Fujii and Ozawa synthesized and thermally decomposed magnesium borohydride [25]. Equation 9 and Equation 11 exhibit the pathway that Equation 8 also follows, where there is an intermediate formation of hafnium borohydride that is not shown. Magnesium borohydride has a metal to boron ratio of 1:2, and its decomposition forms magnesium diboride without excess diborane formation like in Equation 9 [25]. The magnesium diboride was dried as a powder with poor crystallinity.

$$MgCl_2 + 2NaBH_4 \rightarrow Mg(BH_4)_2 + 2NaCl$$

Equation 10 Synthesis of Magnesium Borohydride

$$Mg(BH_4)_2 \rightarrow MgH_2 + 2B + 3H_2 \rightarrow Mg + 2B + 4H_2 \rightarrow MgB_2$$

Equation 11 Thermal Decomposition of Magnesium Borohydride

Dodecaborohydride, a Polyborohydride

Closo-dodecaborohydride, $[B_{12}H_{12}]^{2-}$, is an easily manipulated icosahedral borane that is a common starting material in boron chemistry [38]. Synthesis of closo-dodecaborohydride, $[B_{12}H_{12}]^{2-}$ can be attained with inexpensive starting materials of sodium borohydride and iodine, also avoiding toxic diborane [38]. Equation 12 shows the reduction of sodium borohydride with iodine, under nitrogen. $Na[B_3H_8]$ is an intermediate product that thermally decomposes into sodium dodecaborohydride in Equation 13 [38]. Isolation of the dodecaborohydride is completed by rinsing with water and acidifying with hydrochloric acid to convert the sodium borohydride to boric acid [38]. To incorporate a heavier metal cation, the sodium was replaced with triethylamine in a neutral solution and then reacted with excess cesium hydroxide in boiling water [38]; these steps are shown in Equation 14 and Equation 15.

$$3NaBH_4 + I_2 \rightarrow Na[B_3H_8] + 2NaI + 2H_2 \uparrow$$

Equation 12 Reduction of Sodium Borohydride [38]

$$5Na[B_3H_8] \rightarrow Na_2[B_{12}H_{12}] + 3Na[BH_4] + 8H_2 \uparrow$$

Equation 13 Conversion to Sodium Dodecaborohydride [38]

$$Na_2[B_{12}H_{12}] + 2(C_2H_5)_3N \cdot HCl \rightarrow [(C_2H_5)_3NH]_2[B_{12}H_{12}] + 2NaCl$$

Equation 14 Substitution of Sodium with Triethylamine [39]

$$[(C_2H_5)_3NH]_2[B_{12}H_{12}] + 2CsOH \rightarrow Cs_2[B_{12}H_{12}] + (C_2H_5)_3N + H_2O$$

Equation 15 Substitution of Triethylamine with Cesium [39]

Overview

Hafnium diboride and carbide UHTC have properties, like the formation of a temperature resistant oxidation layer, that are compatible with hypersonic conditions of sharp leading edges. These ceramics can be deposited more easily and faster than traditional methods by pyrolyzing networked polymers.

Polycarbynes can by synthesized via the unstable Wurtz coupling of trisubstituted sp^3 carbon compounds. Ultrasonically dispersed sodium provides more control over the Wurtz coupling. Diborides can be pyrolyzed from borohydride clusters. Dodecaborohydride, in particular, is less temperature sensitive than smaller borohydride clusters and as an anion can easily bond to metal cations. The focus of the following experiments will be on synthesis of diamond-like polycarbynes, without the inclusion of Group 4 metals, and the synthesis of dodecaborohydride to the point of incorporating metal cations.

Chapter 2 Glove Box Refitting and Carbide Experimental

Analytical Equipment

Spectroscopy equipment used were Thermo Scientific Nicolet 6700 FTIR (Fourier Transform Infared transmission) with KBr cards, blank cards were used as background correction; and Bruker Avance 300MHz NMR Spectrometer (^{1}H Nuclear Magnetic Resonance). Elemental analysis used an Exeter Analytical Inc. CE-440 Elemental Analyzer (C, H, and N elemental analysis). Gas Chromatography-Mass Spectrometry (GC-MS) samples were analyzed on a ThermoQuest PolarisQ iontrap using a Phenomenex ZB1 capillary column with a temperature setting of 40°C to 200°C at a rate of 5°C/min. The oxygen sensor for the glove box was a Dräger PAC 3500 O_2 Sensor.

Glove Box Refitting

To an existing VAC DRI-LAB HE Series glove box and existing plastic tubing was replaced with ¾in Stainless Steel 304 pipe. Older rubber gloves were replaced with a new pair and fitted with glove port caps. A vacuum pump was attached to the transfer chamber to evacuate and refill it with the glove box atmosphere to limit oxygen contamination. An oxygen sensor, accurate up to 0.05% by volume moved into the glove box. The system layout is shown in Figure 15. The argon cylinder used to fill up the glove box and adjust the system pressure is shown in Figure 18.

A large balloon was used to refill the glove box. It was filled with argon and pushed the air out through the exhaust. The balloon was then allowed to empty the argon into the glove box and then the process was repeated two more times. Figure 16 shows the inflated balloon in the glove box.

A two part regeneration system that includes 8.3kg Gettermax® 133 Copper-type Catalyst (Research Catalysts, Inc.) layered with 0.5kg 4X10 Mesh Activated Carbon (Strem Chemicals) and 5kg 10Å RCI-DRI 13X Molecular Sieves (Research Catalysts, Inc.) in custom stainless steel cylinders was added with its own recirculation pump to remove any oxygen, solvent or water vapor. Each cylinder was fitted with heating tape with a controller, thermocouples attached the top and bottom of the cylinder, and wrapped in insulating matting. Figure 17 shows the layout of the cylinders. After transferring materials and equipment into the glove box the heating tape was set to 300°F (149°C) and the pump circulated the glove box atmosphere through the cylinders over 12 hours. For a procedure on transferring materials in and out of the glove box see Appendix A.

The cylinders can each be isolated for regeneration and have outlets to let any water released to drain out. A gas mixer is attached to the argon source to bleed in the hydrogen necessary for copper catalyst regeneration. The gas cylinders are attached to the system with rubber hose typically used in welding. The gas mixer can be seen in Figure 18 and a piping and instrumentation diagram is provided in Appendix A.

Regeneration of Molecular Sieve

This procedure was based off of Sigma-Aldrich Technical Information Bulletin AL-143 [40]. With a steady flow of argon, the drain valve on the molecular sieve cylinder, which can be seen in Figure 17, was opened. The temperature of the cylinder's heating tape was set to 400°F (204°C). After the cylinder reached temperature, it was left to purge overnight until there was no more drainable liquid. The temperature controller was shut off and the cylinder was allowed to cool to room temperature before the argon was shut off and the drain valve closed.

Regeneration of Copper Catalyst

The copper catalyst cylinder was preheated with a set point of 325°F (163°C). A flow of 88 scfh (42 slpm) argon with 65 psig (448 kPa) back pressure on the regulator was run for 2hrs with the drain valve open, similar to the one in Figure 17. A 1L flask was used to catch condensate from the drain valve.

Next the temperature set point was increased to 350°F (177°C) and using the gas mixer shown in Figure 18, 2vol% hydrogen gas was added to the argon flow. As a partial regeneration 3 argon cylinders were used over the course of 2 days. After regeneration, the copper catalyst cylinder was purged with pure argon for an additional hour and the temperature controller was turned off. The drain valve could then be closed.

For the illustrated operating procedure see Appendix A.

Carbide Experimental

The experimental method and set-up is based on the procedure outlined by Bianconi et al [11]. Inside the argon-filled dry glove box were an ultrasonic probe and custom thermoelectric cooler, to disperse and cool the reaction, respectively, shown in Figure 19. The design of cooling block is shown in Appendix B, Figure 50. Unless otherwise stated the Autotune Series High Intensity Ultrasonic Processor 750W Model (ultrasonic probe), using a Sonics Vibra Cell controller, was set at 20% amplitude with a pulse of 1sec on and 1sec off, the energy output values are listed in Appendix B,. The thermoelectric cooler is comprised of an aluminum block with a cavity for a reaction vessel partially filled with sand, and 5 cooling units that each has 2 Peltier coolers in series, a heat fin and a fan. The cooling units were connected in parallel and hooked up to a voltage source set at 10V.

Wurtz Coupling of Bromoform

All chemicals, except when stated, were used as purchased. This series of experiments were run with 0.50g NaK alloy, although one run was increased to 5.00g NaK alloy to gauge scalability. In the glove box set-up shown in Figure 19, the NaK alloy was added to 38.2g tetrahydrofuran (THF) and 1.86g dimethoxyethane (glyme) in a 100 mL round bottom flask. Using the ultrasonic probe, the mixture was dispersed for 5min to form a light blue suspension.

In 7.86g of THF, 1.36g of bromoform (97%, Alfa Aesar, distilled with molecular sieve) was added dropwise while still sonicating. It was kept sonicating for half an hour. The suspension turns from light blue to dark grey with dark solids at the bottom of the reaction vessel.

Quenching and Separation

The reaction vessel was brought out of the glove box. It was first quenched with about 10mL methanol and then with 10mL water. The reaction solution turned yellow and white precipitate would form and then dissolve in the aqueous layer during quenching.

The aqueous and organic layers were separated in a separatory funnel. If there was no immediate separation, then a saturated sodium chloride-water solution was added. Sodium sulfate was used to dry the organic layer, which was filtered and then vacuum dried in a rotary evaporator. Any remaining solvent was dried under nitrogen.

If the product was still a liquid, it was mixed in with hexanes to precipitate. These solids were filtered out and dried under nitrogen. ^{1}HNMR ($CDCl_3$): 5.83 (s, C=C-*H*), 5.00 (m, C=C-*H*), 3.58 (m, *H*C-OR), 2.16 (m, *H*C-Br), 1.67 (s, C=C-C*H*$_3$), 1.44 (m, R_3CH), 1.28 (m, R_2CH_2), 0.898 (s, RCH_3). Carbon, hydrogen and nitrogen elemental analysis: C=50.45wt%, H=6.41wt%, N=0.22wt%, R=41.29wt%. A comparison of NMR spectra between literature, 5.0g NaK alloy scale and 0.5g NaK alloy scale is in Table 5. For an elemental analysis comparison see Table 6 and Table 7.

Modifications

Electrolysis

This method was based off of several papers by Nur et al.on electrolysis induced Wurtz coupling [21, 41]. They include two methods, using different salts in the electrolyte solution, for the coupling of chloroform.

Tetrabutylammonium Tetrafluoroborate Electrolyte

In a fume hood in a 5mL test tube; 0.128g tetrabutylammonium tetrafluoroborate was added to 3mL acetonitrile. Stainless steel 6.3mm X 10mm strips were used as electrodes and connected to AA batteries as a volt source. One drop of chloroform was added to the test tube. The electrolysis was started at 1.5v, one AA battery, for half an hour. The voltage was then increased to 3.0v for another half hour. This was repeated to a maximum voltage of 6.0v. Brown solids formed on both the anode and the cathode.

Sodium Chloride Electrolyte

In a fume hood in a 5mL test tube; 3mL acetonitrile was added to 0.014g sodium chloride in 0.5mL deionized water. One drop of chloroform was added to the solution then the stainless steel electrodes were inserted, attached to the 6.0v source. The reaction was sustained for 4 hours. The solution turned red-orange with a dark solid, shown in Figure 14.

Two controls were used for comparison to the sodium chloride electrolyte method. The first control was made without chloroform; the incremental voltage increases occurred every 15min. Brown solids also occurred on the electrodes. The second control removed water from the electrolyte solution, but included the addition of chloroform, and 6.0v sustained for 10min. No visible reaction occurred.

Activated Metal in Silica Gel

The reactions were ran at 0.5g metal (Na and K_2Na) in silica gel (SiGNa Chemistry) and 4g metal in silica gel scales, with the bromoform scaled according to the approximate weight percent of metal deposited in the silica gel. For these reactions 30-40wt% was assumed from value on the MSDS provided by SiGNa Chemistry [42]. Instead of working in an argon-filled glove box, nitrogen flowed through the reaction apparatus while sonicated. The ultrasonic probe had the amplitude set to 25% continuously without pulse.

For 0.5g Na-SG ^{1}HNMR ($CDCl_3$): 1.45 (m, wk, R_3CH), 0.094 (m, Si). For 0.5g K_2Na-SG ^{1}HNMR ($CDCl_3$): 6.85(s, wk, C=C-*H*), 1.58-1.57 (s, br, R_3CH), 1.39-1.20 (s, R_2CH_2), 0.95-0.86 (m, Si). See Table 2 for comparative proton NMR spectra between reaction runs and Table 3 for the comparison with petroleum jelly. Carbon, hydrogen and nitrogen elemental analysis for 0.5g Na-SG: C=32.71wt%, H=6.89wt%, N=0.81wt%, R=59.6wt%. There was a scale-up reaction with 3.3g sodium in silica gel (Na-SG), but it reacted violently when quenched and was not analyzed further.

Solvent Substitution

Two different solvents were tried as alternatives to the THF-glyme mixture, heptane and toluene, matching the molar quantity of the THF used by Bianconi et al.

Heptane

In the glove box set-up shown in Figure 19, in a 100mL round bottom flask 0.5g NaK alloy was added to 30.8g heptane. Using the ultrasonic probe the reaction was dispersed for 5min to form a light blue suspension.

In 5.87g of heptane, 1.36g of bromoform was added. This was added to the blue suspension dropwise while sonication continued for an additional half hour. The mixture turned from light blue to dark grey.

The reaction vessel was brought out of the glove box and quenched with methanol and then water. Tan solids formed during the quench and then dissolved into the dark brown aqueous layer. The top organic layer was clear upon separation.

THF and a saturated NaCl and water solution (brine) were added to the aqueous layer to collect any remaining organic compounds. The new organic layer was vacuum dried. ^{1}HNMR ($CDCl_3$): 6.99 (s, wk, C=C-*H*), 5.01 (s, wk, C=C-*H*), 3.48 (m, *H*C-OR), 2.29 (s, wk, *H*C-Br), 1.45 (s, R_3CH), 1.26 (m, R_2CH_2), 0.0352ppm (s, CH_3). FTIR (cm^{-1}): vC-H 2900, vO=C=O 2300.

Toluene

In the glove box set-up shown in Figure 19, in a 100mL round bottom flask 0.5g NaK alloy was added to 38.86g toluene. Using the ultrasonic probe the reaction was dispersed for 5min to form a light blue suspension.

A solution of 7.40g toluene and 1.36g bromoform was added dropwise to the suspension. This was continuously sonicated for half an hour and turned from light blue to dark grey.

The reaction vessel was brought out of the glove box and quenched with methanol and then water. The quenching formed two cloudy yellow layers. The organic layer was removed and dried with sodium sulfate. THF and brine were added to the aqueous layer to collect any additional organic solids; this new organic layer was separated from the aqueous layer and dried with sodium sulfate. Both organic layers were decanted from the salts and vacuum dried. ^{1}HNMR ($CDCl_3$): 2.34 (s, br, wk, Ar-C-*H*), 2.19 (s, O=C-C-*H*), 0.0951 (s, R-CH_3). FTIR (cm^{-1}): vC-H 3100-2800.

Crown Ether

As a control to observe the solvent behavior without including the Wurtz coupling step complexing agent, 18-crown-6 was used. Then the reaction step was added back in to analyze if the complex to the sonicated emulsion.

Tetrahydrofuran and Glyme

In the glove box set-up shown in Figure 19, with a stir plate and stir bar instead of an ultrasonic horn, 4.68g 18-crown-6 ether was added to 38.2g THF and 1.86g glyme in a 125 mL flask, it was stirred until the crown ether was completely dissolved. Then 0.5g NaK alloy was added to the solution, this was again stirred until dispersion, going from clear to indigo as the complex formed.

After sitting for 24 hours, the solution turned yellow. It was brought out of the glove box and then poured into a plastic container. The solution was basic, with a pH=10. ^{1}HNMR ($CDCl_3$): 3.76-3.67 (m, *H*C-COOR), 3.54 (s, *H*C-OR), 3.39 (s, *H*C-OH), 1.89-1.83 (m, C=C-CH_3), 0.0016 (s, wk, RCH_3 or cyclopropane). Over time the solution turned reddish brown with oxidation.

Heptane and Methyl Naphthalene

In the glove box 4.68g 18-crown-6 ether was added to 30.8g heptane in a 125 mL flask. Then 0.5g NaK alloy was added to the solution, this was sonicated for 4min to force the crown ether to dissolve and complex with the metal.

Since the mixture was clear with suspended alloy, the heptane was poured off and replaced with 110g methyl naphthalene. The complex slowly turned the entire solution violet. Then 4g methylene bromide was added turning the solution dark brown.

Quenching first occurred inside the glove box with ethyl acetate; then the mixture and the removed heptane was brought out of the glove box and quenched with methanol, then water. Ethanol was added to the methyl naphthalene reaction solution to force separation of the organic and aqueous layers, but the mixture stayed in one layer.

Toluene

In the glove box set-up shown in Figure 19, with a stir plate and stir bar instead of an ultrasonic horn, 4.68g 18-crown-6 ether was added to 38.85g toluene in a 100 mL flask, it was stirred until the crown ether was completely dissolved. Then 0.5g NaK alloy was added to the solution, this was again stirred until dispersion, going from clear to black as the complex formed.

Methylene Bromide Addition

To the toluene-crown ether reaction mixture, 1.40g methylene bromide (ACROS Organics) in 7.40g toluene was added, turning the solution reddish brown. It was left to settle to a yellow liquid with brown solids. Ethyl acetate was used to quench the reaction before it was brought out of the glove box.

Once the reaction solution was brought out of the glove box it was vacuum dried until only crystals remained. ^{1}HNMR ($CDCl_3$): 3.67 (s, *H*C-OOCR), 3.45 (s, wk, *H*C-OR), 2.61 (s, wk, *H*C-Br). ^{1}HNMR (DMSO): 3.54 (s, *H*C-OH), 3.30 (s, wk, *H*C-OR), 3.17 (s, wk, RO*H*), 2.50 (m, wk, *H*C-Br).

The solids were dissolved in water and a sample of the product was separated on a Fisher Scientific Marathon Micro A Centrifuge for 10min at the maximum setting. ^{1}HNMR ($CDCl_3$): 3.67 (s, wk, RO-C*H*), 1.55 (s, R_3CH), 1.28 (s, wk, R_2CH_2), 0.0254 (s, RCH_3 or cyclopropane).

1,10-Dichlorodecane Addition

To the toluene-crown ether reaction mixture, 1.70g 1,10-dichlorodecane (Aldrich) in 7.40g toluene was added, turning the solution brown. It was brought out of the glove box and quenched with methanol and water. The organic layer was separated and dried with sodium sulfate. Then the organic layer was filtered and vacuum dried. ^{1}HNMR ($CDCl_3$): 7.41-7.18 (m, Ar-*H*), 3.76 (m, *H*C-OR), 3.60 (m, *H*C-Cl), 2.69 (m, wk, *H*C-C=O), 2.44 (s, Ar-C*H*), 1.84 (m, wk, C=C-CH_3), 1.58-1.27 (m, R_2CH_2), 0.97 (m, RCH_3).

Bromoform Addition

To the toluene-crown ether reaction mixture, 1.36g bromoform in 7.40g toluene was added, turning the solution dark brown with black solids. It was brought out of the glove box and quenched with methanol and water. The solids were filtered out and rinsed with methanol. The light yellow organic layer was separated and dried with sodium sulfate. Then the organic layer was filtered off of the salts and vacuum dried. ^{1}HNMR ($CDCl_3$) Organic Layer: 3.60 (s, *H*C-OR), 2.94 (s, wk, C=C-C*H*$_3$), 1.27 (s, wk, R_2C*H*$_2$). ^{1}HNMR ($CDCl_3$) Solids: 3.69 (s, HC-O*H*), 3.50 (s, C*H*$_3$-OH), 1.10 (s, br, wk, R_2C*H*$_2$).

Bromobenzene Addition

To the toluene-crown ether reaction mixture, 2.53g of bromobenzene was added, turning the solution reddish brown with black solids. It was brought out of the glove box and quenched with methanol and water. A separatory funnel was used to remove the aqueous layer from the organic layer. The organic layer was dried with sodium sulfate, filtered then vacuum dried. ^{1}HNMR ($CDCl_3$): 7.58 (m, Ar-*H*), 4.06 (m, wk, *H*C-Br), 3.75 (m, wk, *H*C-OR), 2.42 (m, wk, R_2-C*H*$_2$). GC-MS data is provided in Table 13 in Appendix C.

2-Bromotoluene Addition

To the toluene-crown ether reaction mixture, 2.76g of 2-bromotoluene was added, turning the solution orange-red with black solids. It was brought out of the glove box and quenched with methanol and water. A separatory funnel was used to remove the aqueous layer from the organic layer. The organic layer was dried with sodium sulfate, filtered then vacuum dried. GC-MS data is provided in Table 14 in Appendix C.

Chapter 3 Carbide and Glove Box Results

Electrolysis and Activated Metal in Silica Gel

Since the glove box required significant repairs and updates, electrolysis and active metals in silica gel were tried as alternatives. If they had been successful methods then using the cumbersome glove box would have been avoided.

Electrolysis

Nur et al. [21, 41]claim their electrolysis method to be "facile," and though the set-up is easy, the rigor of their research could be increased [43]. The amount of reaction material in comparison to supporting electrolyte solvent is very small, which is not reasonable for scale-up. Their proposed reactions are shown in Equation 16, provided by Sizov et al. Work by Sizov et al. focuses on ball milling the reactants to form the poly(hydridocarbyne) powder [43]. Since here the application is for polymer preceramic coatings the method by Sizov et al. was not used.

$$RCCl_3 \xrightarrow[-Cl_2]{i} [RCCl_m]_n \xrightarrow{ii} (CR)_n$$

R = H, Alk, Ar.

i. Acetonitrile, supporting electrolyte, electrolysis; *ii*. THF, $LiAlH_4$.

Equation 16 Proposed Reactions by Nur et al. via 6v Potential [43]

Over the course of these reactions, noticeable pitting occurred on both electrodes. The red-orange solids that formed were insoluble in common organic solvents, and can be assumed to be iron oxide forming from the electrodes. An example of the reaction set up is in Figure 14.

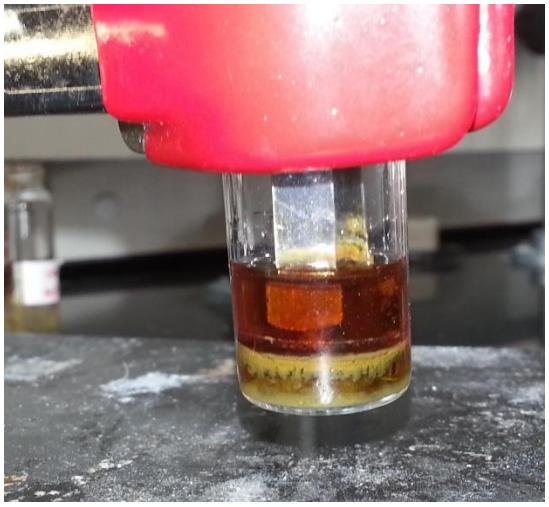

Figure 14 Sodium Chloride Electrolysis Reaction with Chloroform

Minimal gas was generated, but not analyzed. The standard half-cell potentials of all components in these reactions are below 6.0v at room temperature, even the conversion of fluorine to fluoride is at +2.866v [44]. This means that there is a possibility that anions from the salts were converting to their gaseous state, especially at the higher voltages. Since the reaction was independent of chloroform, the sp^3 carbon source, and the safety risk of halogen gas generation these reactions were not continued.

Activated Metal in Silica Gel

During glove box repairs and when completely inert systems were unavailable, sodium and sodium potassium alloy (K_2Na) in silica gel (SG) were tested as less sensitive alternatives to these active metals. Since silica gel is porous, metals deposited in the pores are more removed from the atmosphere, but can still react when in a solvent [45]. Note, that though sodium in silica gel was effervescent in water, like stated in literature, the K_2Na alloy in silica gel had a red glow when exposed to air [45]. Also, due to the nature of the pores, the metals have a high surface area to volume ratio, so will not lose reactivity in a solvent.

For both sodium in silica gel at the 3.3g scale and K_2Na alloy in silica gel at the 4g scale, after the addition of bromoform, the solution was very reactive to the quenching step, more so than at the smaller scale reactions. The proton NMR spectra of these reactions, shown in Table 2, were not consistent with scaling, nor were they similar to data provided by Bianconi et al. [11]. The wash with dichloromethane was meant to remove any residual reaction solvent from the product; the difference in peaks is not due to the presence of dichloromethane [46]. The peaks near 0.0ppm most likely represent silicon [46], which also contributed to the 59.6wt% residual value of the elemental analysis.

0.5g Na-SG	**0.5g K_2Na-SG**	**0.5g K_2Na-SG After a CH_2Cl_2 Wash & Dried**	**4g K_2Na-SG**	**Bianconi et al.** [11]
			s 6.85ppm	
			d 2.48ppm	
s, wk 1.45ppm	s 1.58ppm		d 1.56ppm	s 1.59ppm
	s 1.27ppm	s 1.28ppm		s 1.25ppm
	m 0.92ppm	s 0.92ppm		
s 0.094ppm	s 0.17ppm	s 0.17ppm		
		s, wk 0.12ppm		

Table 2 ^{1}HNMR Comparison of Metal in Silica Gel Experiments with $CDCl_3$ as the Solvent

The 0.5g K_2Na-SG product NMR spectra were also compared to white petroleum jelly in Table 3, as petroleum jelly contains higher molecular weight hydrocarbons. The proportions of peaks were measured against the common 1.24ppm peak. The lack of the 1.50ppm peak in the dichloromethane-washed product and the dominant presence of the 1.24ppm peak indicate that the majority of the product, like the petroleum jelly, is secondary carbon chains.

Approx. Peak	Vacuum Dried Solids	CH_2Cl_2 Washed	Petroleum Jelly
1.50ppm	0.3	-	0.1027
1.24ppm	1	1	1
0.85ppm	0.3132	0.2825	0.2726

Table 3 ^{1}HNMR Peak Proportionality Comparison of K_2Na-SG Products vs Petroleum Jelly

Due to the inconsistent proton NMR when the reaction was scaled and the possibility that the silica gel was being digested and releasing some metal unreacted, this method is not recommended for further study.

Glove Box Refitting

To keep the reactions dry and in an oxygen-free environment, a glove box was moved into the lab and its piping and support equipment replaced to reduce possible leak locations, Figure 15 shows the glove box details. Glove port caps were built to allow gloves to be removed without compromising the glove box environment [47]. The oxygen sensor, designed for use in air, measures the efficacy of the regeneration system by reading the oxygen levels in the glove box. Occasionally the oxygen sensor would trigger its high alarm in the dry glove box; this could have been due to argon affecting the sensor. Allowing the sensor to sit in air for several weeks typically returned the sensor to its working state. It is recommended that oxygen sensors be removed from an argon-filled glove box in between use.

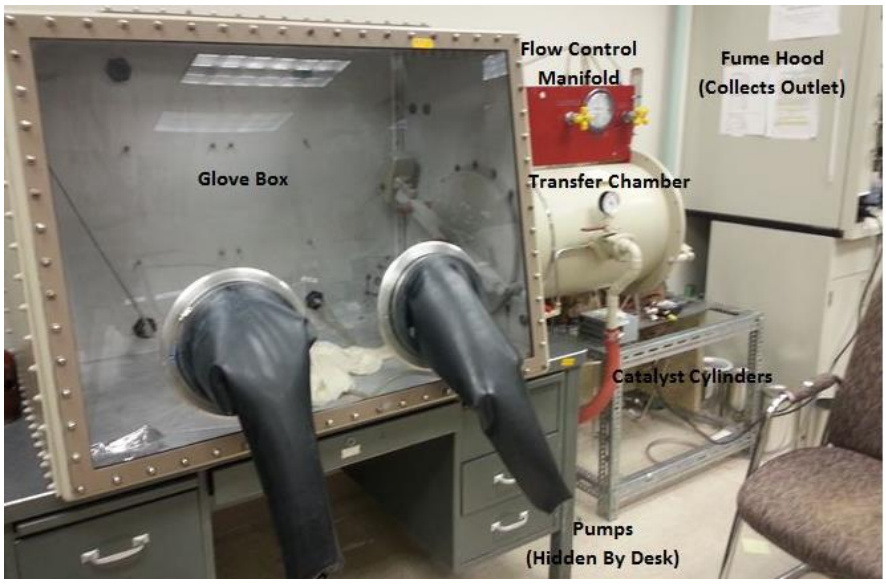

Figure 15 Glove Box System

The balloon used in filling the glove box with argon, shown in Figure 16, proved to be a very effective method to force air out of the system without letting oxygen mix with the incoming argon. The glove box only had to be refilled three times to reduce the oxygen content to read 0.0vol% on the oxygen sensor.

Figure 16 Balloon in Glove Box

Regeneration of Molecular Sieve

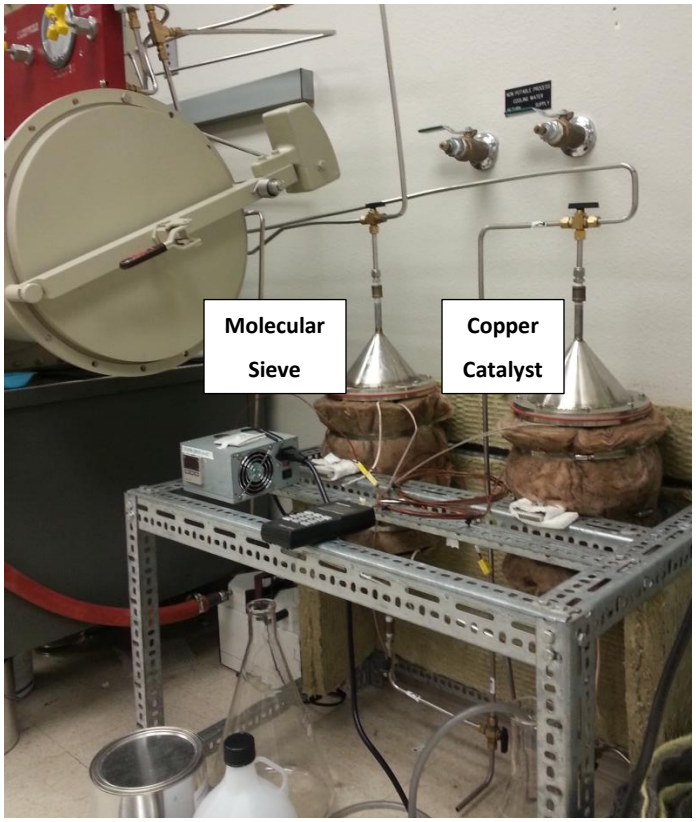

Figure 17 Detail of Regeneration System

Using 13X molecular sieves as opposed to 4Å molecular sieves allows the removal of a wider range of organic solvents in addition to water vapor from the glove box system [40, 48]. Regeneration of this cylinder was straightforward and water condensation was removed during its cycle; when there was no more water vapor generated the regeneration was complete.

The need for a nearly redundant deoxygenation system as the copper catalyst protects the catalyst, as the reaction between oxygen and the catalyst is exothermic and can cause overheating during regeneration that reduces its lifetime [47].

Regeneration of Copper Catalyst

Copper catalyst is able to be used to remove oxygen at higher temperatures and allows for a large number of removal cycles before it needs to be regenerated [48]. The combination of activated carbon and copper catalyst in this cylinder removed impurities and decomposition products in the system [48]. The carbon black needs no extra regeneration step as it will start to regenerate when the system reaches 392°F (200°C) and will be fully regenerated after 24hr [47].

To completely regenerate the copper catalyst cylinder 10 cylinders of argon are needed, if the gas mixer was not installed, this would have been 10 cylinders of the mixed gas. Still, only three argon cylinders were used. The gas mixer is shown in Figure 18.

Figure 18 Detail of Gas Mixer

Appendix A includes the operating procedure for regenerating the copper catalyst system, based on information provided by Research Catalysts, Inc., however there was a large observed temperature drop along the height of the cylinder. The temperature controller during regeneration is connected to the bottom thermocouple and the second thermocouple, located at the top of the cylinder, is connected to a measurement device. Table 4 shows an example of temperature zones inside of the cylinder when using a third thermocouple probe. Note that the top is significantly lower, however, because the internal temperature readings were performed with the lid off of the cylinder.

Top	
Center	Side
288°F	329°F
Middle	
Center	Side
395°F	436°F
Bottom	
Center	Side
324°F	335°F

Table 4 Copper Catalyst Cylinder Temperature Profile, Set Point=325°F

Based on literature provided with the copper catalyst the maximum recommended temperature is 437°F (225°C), though short term temperature spikes of 527-572°F (275-300°C) can be endured with limited damage [49]. Before temperature readings were made internal to the cylinder, the controller set point was as high as 500°F (260°C), which could degraded the catalyst, especially along the side wall. At the time there was 5kg of catalyst in the cylinder, then, to refresh the catalyst, about 1kg of the catalyst was replaced with 4.4kg of new catalyst before regeneration was attempted at lower temperatures.

Wurtz Coupling, Quenching and Separation

Miller et al. [14] make note of the importance of some type of cooling for Wurtz-type reactions, as they found that for non-steric hindered monomers, the reactions could be violently exothermic. The decision to use the modified cooling block, shown in Figure 19, instead of liquid cooling was due to possible contamination of the glove box atmosphere or reaction with the NaK alloy, which would interfere with the reaction.

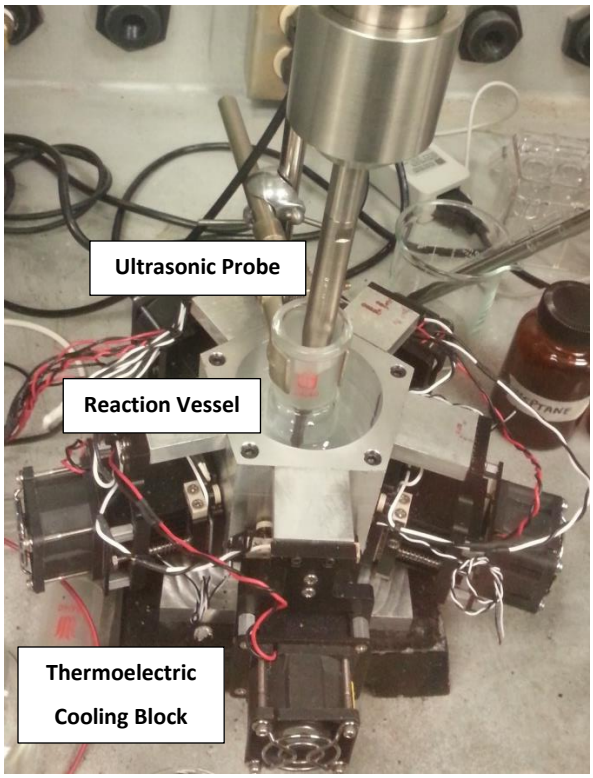

Figure 19 Sonication and Cooling Apparatus

The emulsion of the metal into solvent formed the light blue colored emulsion as shown in Figure 20, this was later found to be solvent independent.

Figure 20 NaK Emulsion in THF/Glyme

Consistency of the reactions at different scales was also tested, especially since the previous reactions with metal in silica gel tended to degrade the silica gel at larger experimental volumes. When following the Bianconi et al. method the reactions yielded relatively consistent proton NMR spectra, comparison shown in Table 5, between the 5 g scale and the 0.5 g scale, but the product proton NMR results had more peaks than Bianconi et al [11]. This could possibly be due to the degradation of the solvents: tetrahydrofuran and glyme, which both have peaks in the 2.00 ppm to 4.00 ppm range [46].

5 g Scale Run #1	**0.5 g Scale Run #1**	**Bianconi et al.** [11]
s 5.83 ppm	s 5.83 ppm	
s 5.01 ppm	m 5.00 ppm	
s 3.70 ppm	m 3.58 ppm	
m 2.19 ppm	m 2.16 ppm	
s 1.67 ppm	s 1.67 ppm	s 1.59 ppm
	m 1.44 ppm	
s 1.28 ppm	m 1.28 ppm	s 1.25 ppm
s 0.927 ppm	s 0.898 ppm	

Table 5 ^{1}HNMR Comparison with $CDCl_3$ as the Solvent

The occurrence of proton NMR peaks at less than 1.0ppm could either identify the hydrogen on a tri-substituted carbon or cyclopropyl groups, like on short chain ivyvanes [50]. Some of the peaks in that range were in proportion with the $CDCl_3$ solvent peak and could be assumed to be from the 0.03% tetramethyl silane (TMS) in some of the solvent used, which shows up as a single peak near 0.0ppm in nearly equal proportions to $CDCl_3$ [46]. The baseline spectra of the $CDCl_3$ is shown in Figure 21 and also includes a small contamination of water at 1.54ppm, which sometimes overlaps with the $–CH_2–$ (secondary sp^3 carbon) peaks. Unlike the activated metal on silica gel experiments, the Bianconi et al. based experiment and the later modifications do not otherwise introduce silicon. The structure of ivyvanes is shown in Figure 22. How ivyvanes will affect conversion to carbide during pyrolysis will need to be investigated further, but it does affect the macromolecular network.

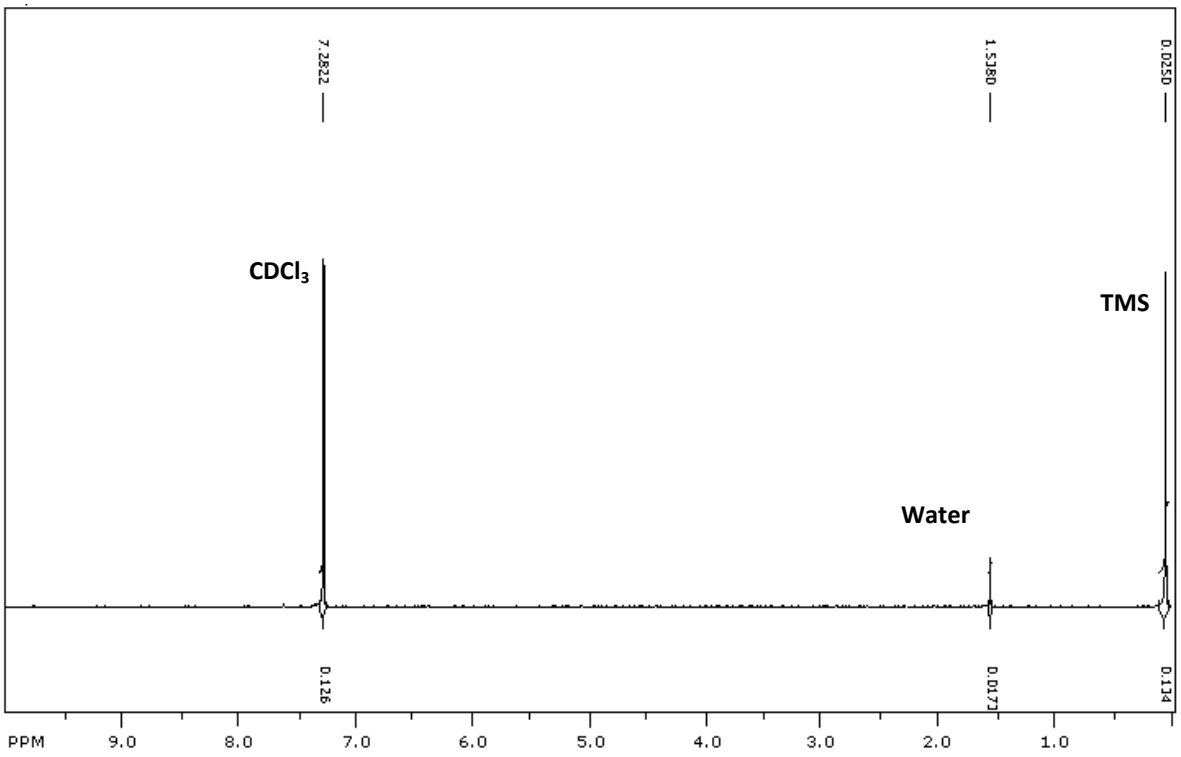

Figure 21 ^{1}HNMR Spectra of $CDCl_3$ with Trace TMS

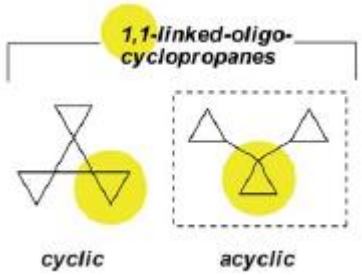

Figure 22 Ivyvane Structure (In Dotted Box) [50]

For additional confirmation that the experimental products were similar at different scales, and to clarify possible contaminants, elemental analysis was done for carbon, hydrogen and nitrogen with the remaining material classified as "R". For samples of about 2mg the weight fraction of each species including the unknown R were given. Table 6 contains the results for the 5g scale product and Table 7 shows the 0.5g scale results, these values are in agreement with multiple samples.

The species represented by R could only reasonably be oxygen or bromine, and was extrapolated out based on the compositions of the ether solvents and the halogenated reactants. Assuming that hydrogen would be bonded to either carbon or oxygen, the amount of moles attributed to being in a C-H bond was subtracted off of the total and the remainder was attributed to an O-H bond. Also assuming that there were no double bonded oxygen present and could only be bonded as C-O-H, the remaining R was attributed to unreacted bromine. If the sample were to be completely reacted without oxygen, the carbon to hydrogen molar ratio would be 1:1.

5.0g Scale			
Element	Weight Fraction	Mole Fraction	Empirical Formula
C	0.5833	0.3866	0.7853
H	0.0619	0.4923	1.0000
N	0.0027	0.0015	0.0031
R=Br	0.1394	0.0139	0.0282
R=O	0.2127	0.1057	0.2147

Table 6 Elemental Analysis of 5.0g Scale Product

0.5g Scale			
Element	Weight Fraction	Mole Fraction	Empirical Formula
C	0.5045	0.3256	0.6559
H	0.0641	0.4965	1.0000
N	0.0022	0.0012	0.0025
R=Br	0.0610	0.0058	0.0117
R=O	0.3588	0.1709	0.3441

Table 7 Elemental Analysis of 0.5g Scale Product

With the low calculated values of bromine, the reaction seems to be reaching completion of using up the active metal and forming bromine salts. However with the presence of oxygen in the product means the possibility that the ether solvents, both THF and glyme, are interfering with the coupling in the reaction. Organoalkali compounds can form at room temperature by the rupture of ethers by NaK [51]. These adducts that form behave as strong bases [51].

It is noted that, according to Miller et al., in the Wurtz coupling of alkylsilanes addition of up to 30vol% diglyme, or other dipolar aprotic solvents, increases yield, but also decreases molecular weight [14]. It is unclear whether the glyme behaved in this manner or formed an organoalkali compound with NaK. Crown ethers were also shown to increase yields [14].

Modifications

Modifications to the Bianconi et al. method were made, first, to adjust to lab conditions, then to identify and remedy side reactions. After the glove box was able to be used and results from the Bianconi et al. method were analyzed, the experiments were repeated without the halogenated reactant due to anomalies when comparing to data from Bianconi et al. This led to substituting different solvents and then adding 18-crown-6 ether, a complexing agent.

Solvent Substitution

Heptane

Initially the system behaved similarily to using THF and glyme as a solvent, a light blue emulsion of NaK alloy in heptane, and the addition of reactant turned the solution a dark brown. The lack of solids in the heptane organic layer suggested that the product was not soluble and therefore could not allow for the continued polymerization during sonication, this was shown by the bromomethane, methylene bromide and bromoform peaks in Figure 23. There were also some short chain oligomers as shown by the strong linear carbon peak at 1.45ppm. The broad oxygenated peak at 3.48ppm was most likely due to additional water contamination leftover from quenching. In the FTIR spectra, shown in Figure 24, there is a strong CO_2 peak in addition to the C-H peak; this was probably due to how little product was available to be deposited on the sample card. The Wurtz coupling experiments on polysilanes done by Miller et al. also indicated increased yield and molecular weight of the product when the product was soluble in the solvent [14]. This solvent does not appear to be suitable to Wurtz coupling as a substitute for THF and glyme.

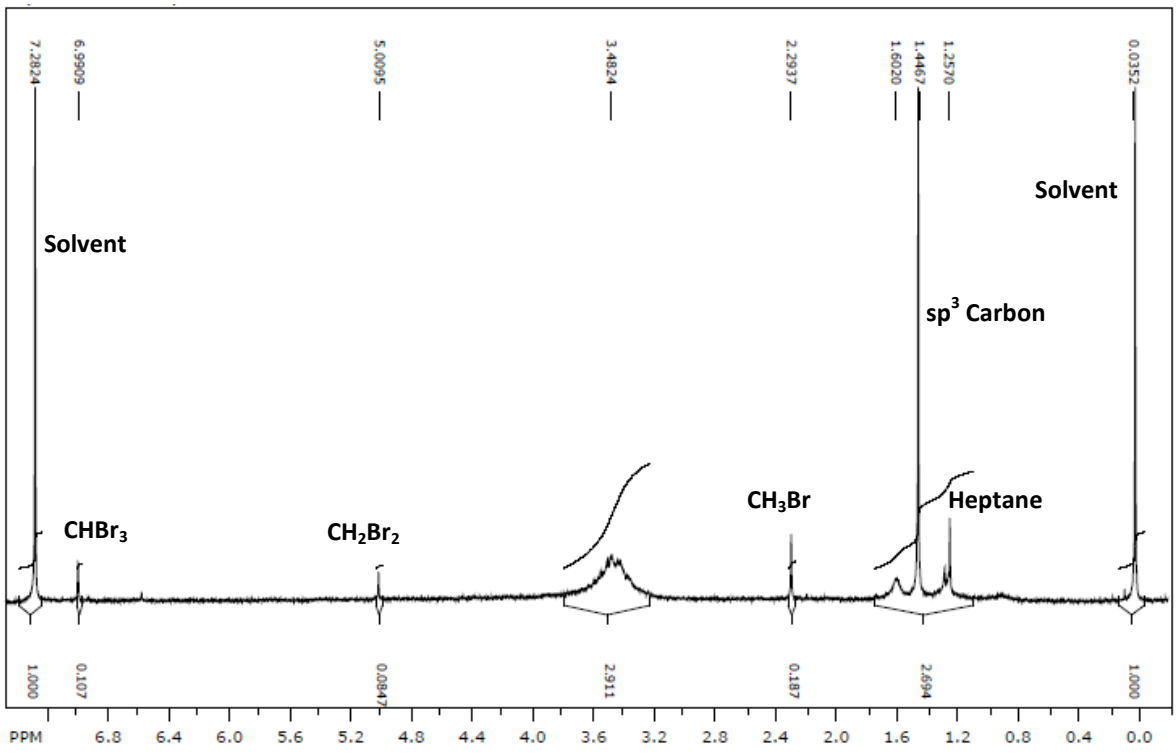

Figure 23 ^{1}HNMR Spectra of Wurtz Coupling in Heptane

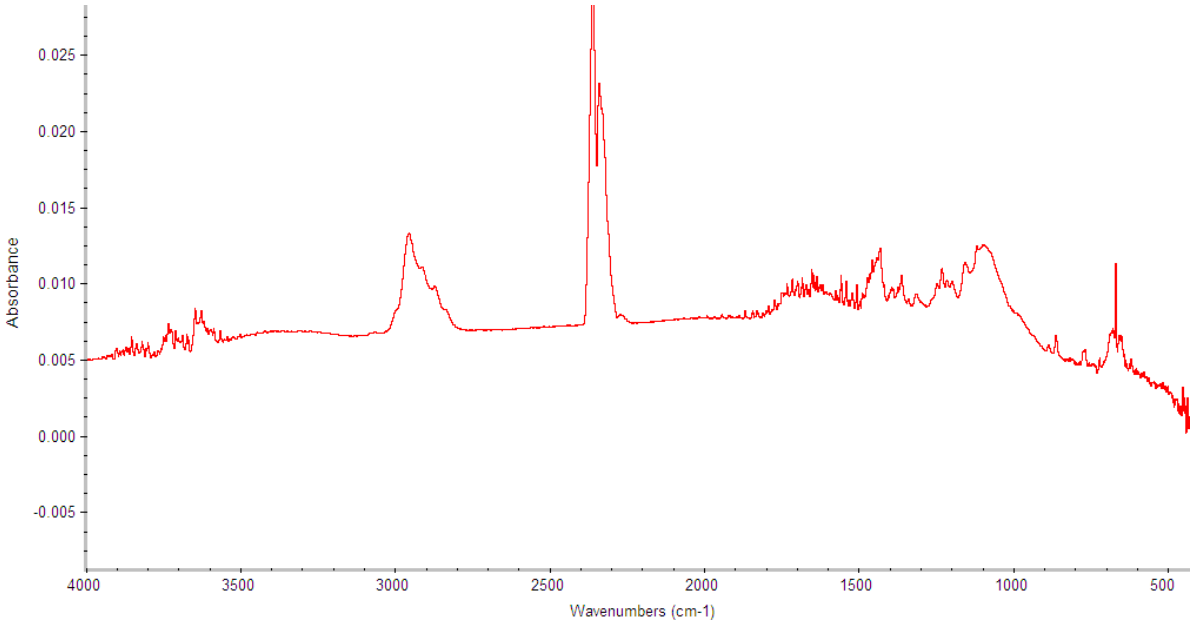

Figure 24 FTIR Spectra of Wurtz Coupling in Heptane

Toluene

Toluene, unlike heptane, yielded a solid product isolated in the toluene organic layer, leading the toluene to be used in the subsequent experiments. However, this solid product is hard to dry and separate from the solvent and as seen from the NMR spectra in Figure 25 may actually be chemically bonded in the polymer. The peaks around 2.19ppm and 2.34ppm are indicative of toluene and acetone, with the broader peak possibly from incorporated toluene and the acetone was used to move the sample to smaller vial after being dried. The toluene IR results were indicative of THF used to apply the sample to the IR card, even after drying for several days; Figure 26 shows the drier FTIR spectra. A precipitation step in no more than 20mL of hexanes is the best method of removing the toluene from the product.

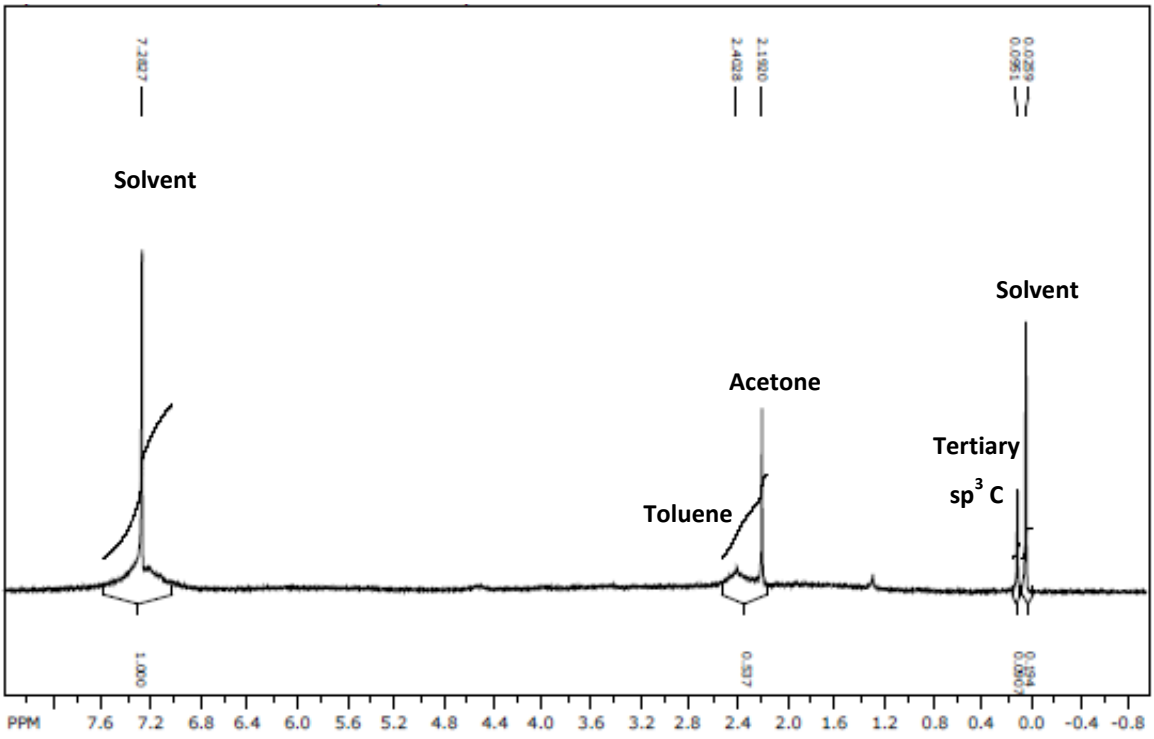

Figure 25 ^{1}HNMR Spectra of Wurtz Coupling in Toluene

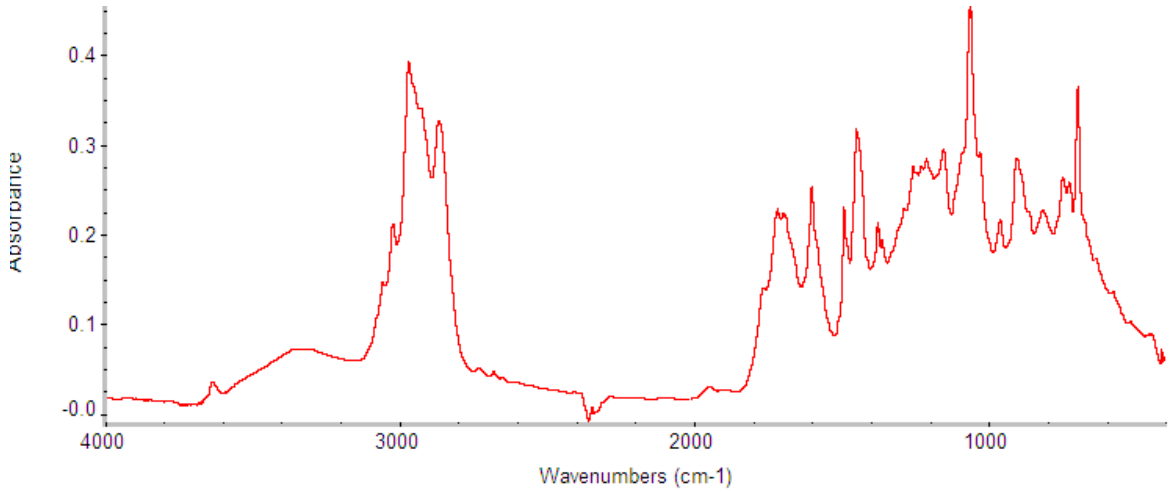

Figure 26 FTIR Spectra of Wurtz Coupling in Toluene

Crown Ether Solvent Substitutions

These mixtures were stirred rather than sonicated since the complex dispersed on a similar scale to the sonicated emulsion, and Miller et al. found it to be effective with their studied substituted dichlorosilanes [14]. Figure 27 shows the structure of 18-crown-6 ether used. Sonicating the crown ether complex during the addition of the brominated reactant did not make a significant difference to the reaction.

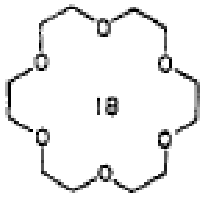

Figure 27 Structure of 18-Crown-6 Ether [52]

Tetrahydrofuran and Glyme

The color change of indigo to yellow implies a lack of stability in the THF-glyme-crown ether solution; this was verified by the basic pH without quenching. The basic pH indicates the formation of the alkoxide hydroxide compound [51].

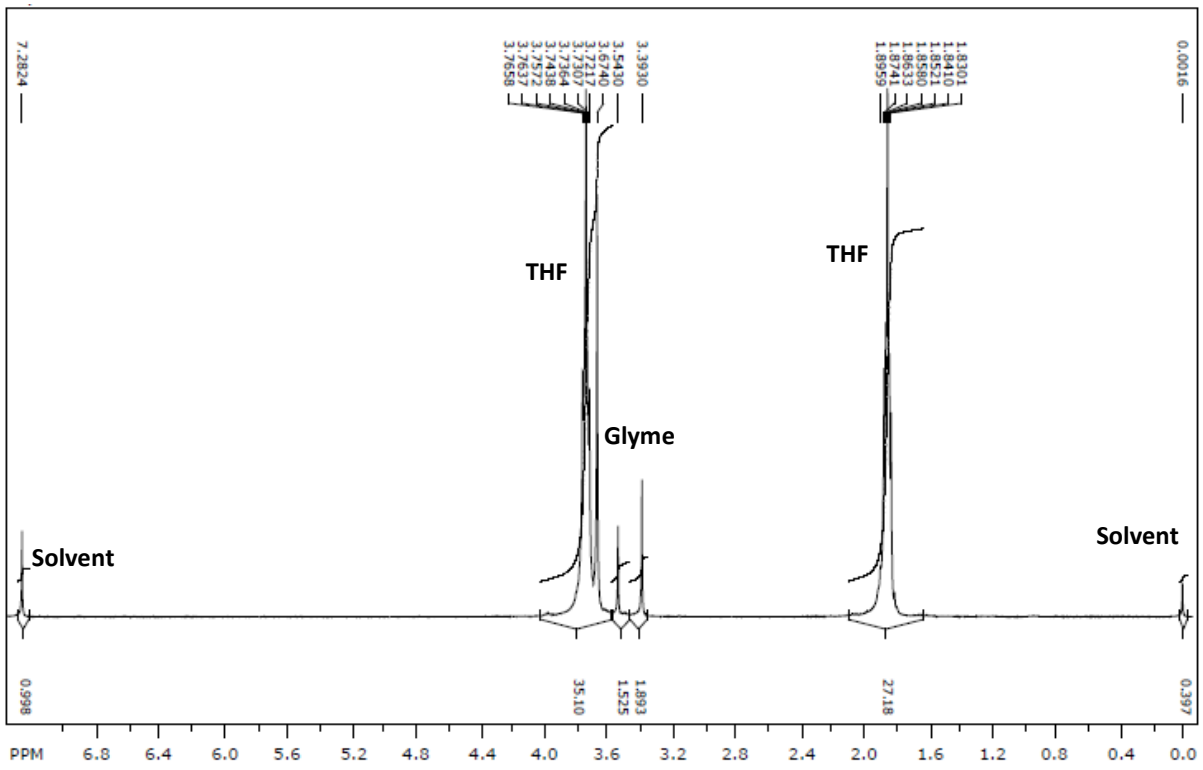

Figure 28 ^{1}HNMR Spectra of NaK and Crown Ether in THF/Glyme

Figure 29 shows the indigo of the forming complex coming off of the spherical droplets of NaK. In Figure 30 the NaK has almost fully complexed and is starting to form a tan side product within hours of the addition. Figure 31 shows the mixture the next day. The proton NMR, in Figure 28 showed a mix of THF, glyme, and decomposition peaks overlapping [53]. This is in agreement with the earlier assumption of the presence of oxygen in the elemental analysis of the sonicated reactions and the complexed NaK alloy will react with the ether solvents. Even in this method, THF and glyme are not recommended for further study.

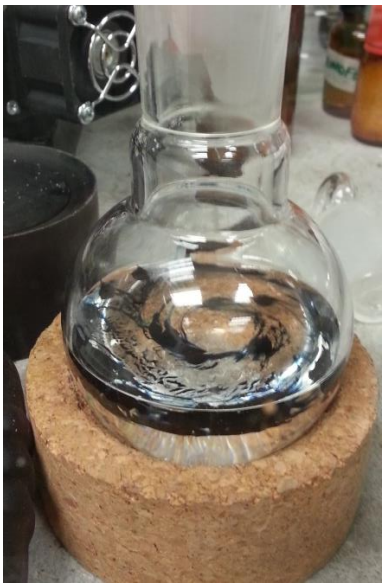

Figure 29 Addition of NaK to 18-Crown-6 in THF/Glyme

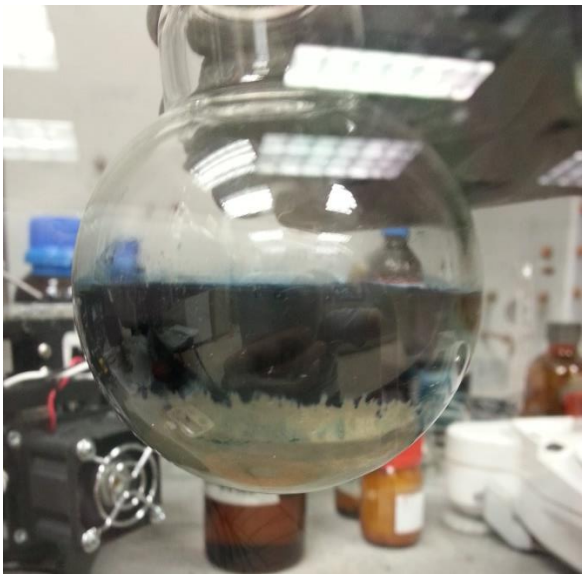

Figure 30 NaK and 18-Crown-6 in THF/Glyme After Agitation

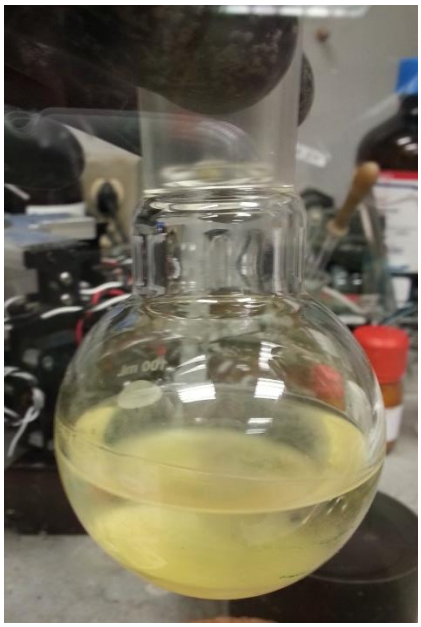

Figure 31 NaK and 18-Crown-6 in THF/Glyme After 24hr

Crown Ether and Toluene Reactions

Crown ether complexed with NaK alloy was very stable when dissolved in toluene. The mixture was able to stay black over several days, as shown in Figure 32. Heptane did not readily dissolve the crown ether, the complex was unable to form and disperse as shown in Figure 32. Once heptane and the THF/glyme mixture were no longer considered for the Wurtz coupling reactions several different reactants were tested using the 18-crown-6 ether and NaK complex in toluene: methylene bromide, 1, 10-dichlorodecane and bromoform. Both methylene bromide and 1, 10-dichlorodecane are bisubstituted and should form similar polyethylene-like polymers, though the dichlorodecane-based polymers would most likely be higher in molecular weight.

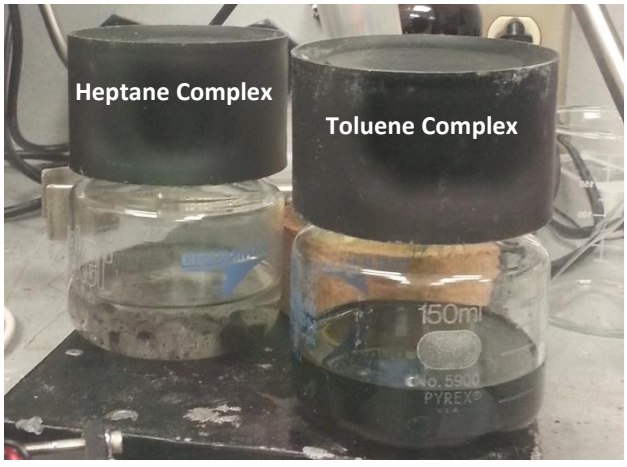

Figure 32 NaK and 18-Crown-6 in Heptane and Toluene (L to R)

Methylene Bromide Addition

Brominated reactants were scaled based off of a 1:1 ratio between the activated metal and bromine ions. To test if Wurtz coupling was capable of occurring with a complexed active metal, methylene bromide was used as the halogenated reactant instead of bromoform.

Methylene bromide has two bromine ions compared to bromoform and would be expected to form oligomers of polyethylene chains upon Wurtz coupling. Polyethylene is not soluble in water, but 18-crown-6 is and there is a large mass difference between the product and the crown ether, so centrifuging was chosen as the separation technique. The proton NMR from the pellet collected from the centrifuge shows evidence of straight-chain alkanes at 1.28ppm and traces of the crown ether at 3.67ppm. Figure 33 shows the pellet spectra. The pellet is shown in a 2mL vial in Figure 34.

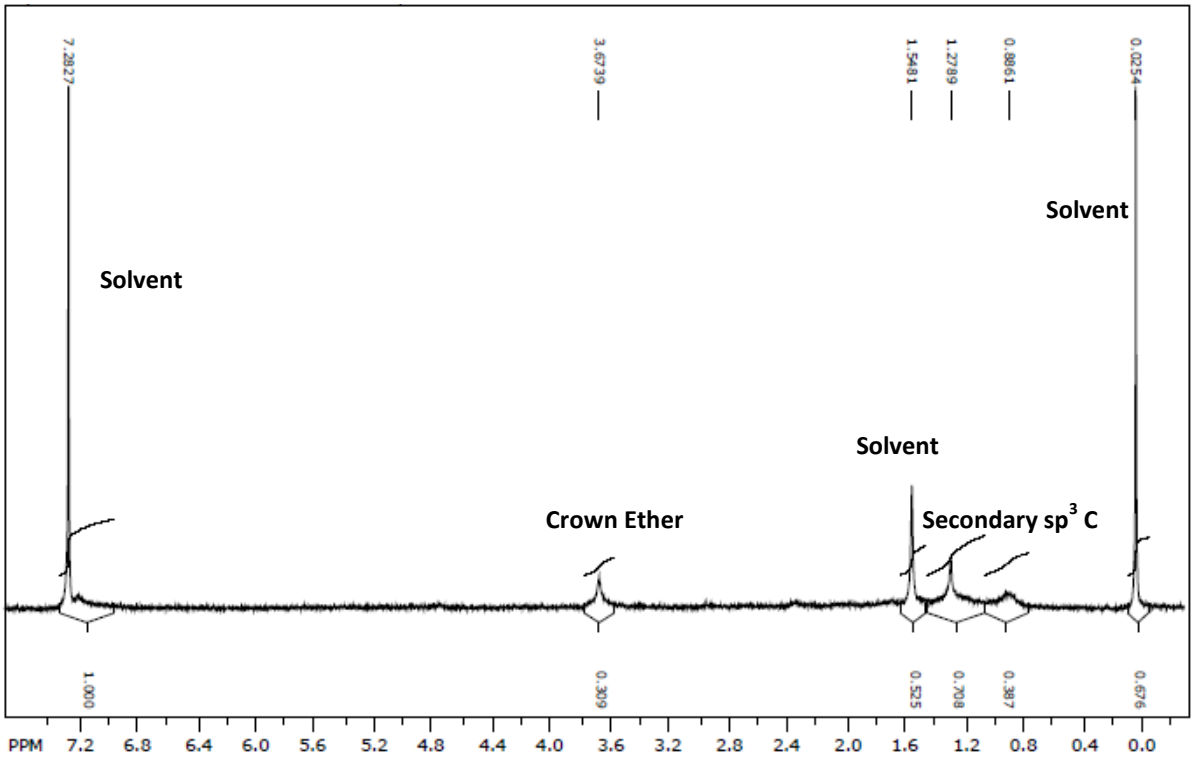

Figure 33 ^{1}HNMR Spectra of Methylene Bromide Addition After Centrifuge

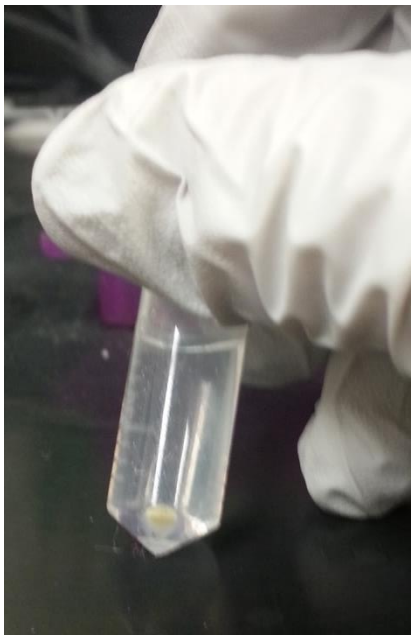

Figure 34 Pellet from Methylene Bromide and Crown Ether in Toluene

1, 10-Dichlorodecane Addition

Since no solids precipitated during the vacuum drying step, with about 10mL of the liquid organic layer left, the proton NMR sample was taken with the liquid. The dominant peaks correspond to toluene, at 7.41ppm-7.18ppm, which also corresponds to the solvent peak, and at 2.44ppm. Peaks that correspond to the dichlorodecane are located at 3.60ppm and the 1.58ppm-1.27ppm range, which could also be the oligomers formed from Wurtz coupling [53]. A slight overlap at 3.76ppm could be due to residual crown ether. The identified peaks are shown in Figure 35. There is a possibility that the peak in the 1.58ppm-1.27ppm range could be cyclodecane, but the peaks at 0.97ppm are indicative of end groups in the straight chain [53].

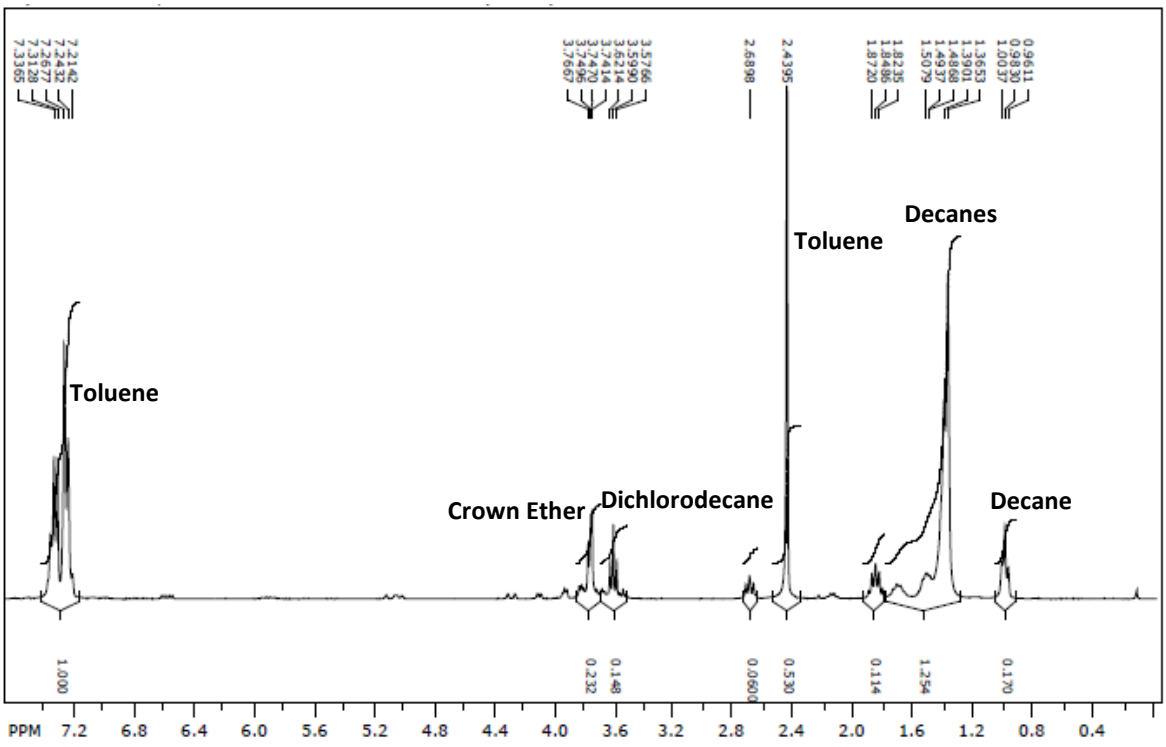

Figure 35 ^{1}HNMR Spectra of 1, 10-Dichlorodecane Addition

Bromoform Addition

The dark solids that formed from the reaction were able to be filtered out of both the aqueous and organic phases. The organic layer was separated and vacuum dried. For consistency NMR spectra were taken of the organic layer, shown in Figure 36 and the solids, shown in Figure 37. There was no presence of tertiary sp^3 bonded carbon in this system as there was in the sonicated NaK-toluene emulsion system with bromoform reactant. Instead there was a strong crown ether peak at 3.60ppm and some toluene and small carbon chains that were mostly driven off while the product was dried. In the solids the dominant peaks between 3.70ppm (indicative of O-H) and 3.50ppm (indicative of C*H*-OH) were from the methanol wash. This means that the emulsion systems should be revisited, as the Wurtz Coupling of bromoform was the most complete in the NaK-toluene emulsion. However, a solvent similar to toluene, but more inert to coupling, like benzene, should be looked at for a purer sp^3 cross-linked product.

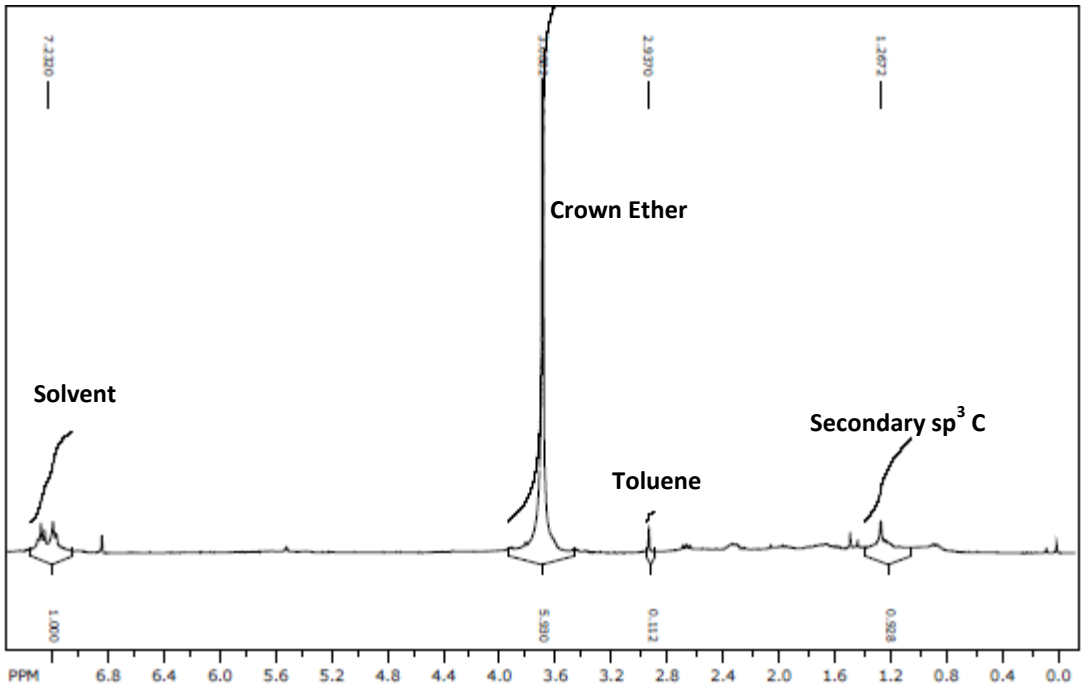

Figure 36 ^{1}HNMR Spectra of Bromoform Addition Dried Organic Layer

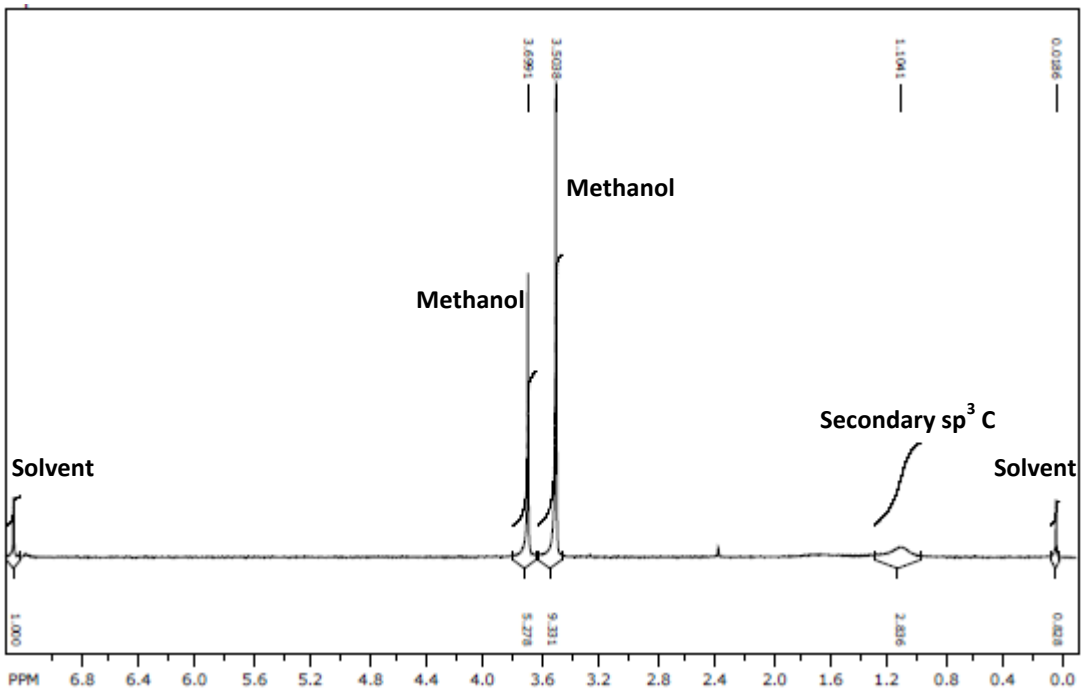

Figure 37 ^{1}HNMR Spectra of Bromoform Addition Solids

Bromobenzene and 2-Bromotoluene Addition

Bromobenzene and 2-bromotoluene were used as reactants to further study the toluene and 18-crown-6 system. The bromobenzene product NMR spectra showed overlapping peaks in the solvent region around 7.6-7.2ppm, this indicates the aromatic ring in bromobenzene as well as any coupling occurring between bromobenzene and possibly toluene. GC-MS was used for identifying the compounds found in the dried product, looking at both the bromobenzene reaction, shown in Table 13 in Appendix C and the 2-bromotoluene reaction, shown in Table 14 also in Appendix C.

In the bromobenzene product there was bromobenzene left, as well as biphenyl (in Figure 38), the expected dimer. However there was also the presence of methyl biphenyls and bibenzyl (in Figure 39), with the extra methyl group indicating the inclusion of toluene in the dimer. Trimers of bromobenzene and toluene formed either chain-like as 2-benzyl biphenyl or dendrimer-like as triphenylmethane.

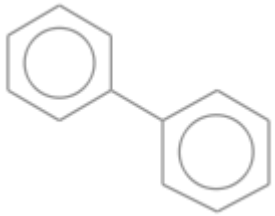

Figure 38 Biphenyl Structure [54]

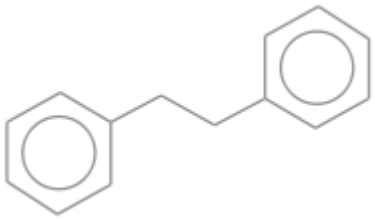

Figure 39 Bibenzyl Structure [54]

In the 2-bromotoluene product, the reactant was also leftover. There were similar methylated dimers as the bromobenzene, like bibenzyl as well as 1-methyl-4-(phenylmethyl) benzene (Figure 40). Overall there were less varied products due to 2-bromotoluene having a similar structure to the solvent.

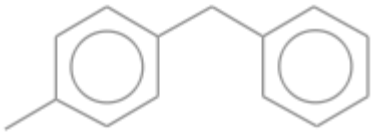

Figure 40 1-methyl-4-(phenylmethyl) Benzene Structure [54]

Chapter 4 Boride Experimental

Analytical Equipment

Nuclear Magnetic Resonance (NMR) Spectroscopy equipment used were Bruker Avance 300MHz NMR Spectrometer (^{1}HNMR) and Bruker Avance 500MHz NMR Spectrometer (^{11}BNMR).

Boride Experimental

Formation of Sodium Dodecaborohydride

The experimental method and set up followed the procedure outlined by Geis et al [38] and Komura et al. [39]. A slurry of 9.93g $NaBH_4$ (98%, Oakwood Products) in 46mL diglyme was heated in a round bottom flask in a sand bath under nitrogen to 95°C. With an addition funnel 24.8g Iodine in 60mL of diglyme was added dropwise to the slurry. It was left to stir for an hour. The heat was turned up to 162°C and refluxed for 16 hours.

Substitution of Sodium to Triethylamine Cation

After the solution was cooled the solvent was distilled off to leave a white solid. This solid was dissolved in about 60mL of water, producing heat and vapor to form a brown solution. About 14mL of concentrated hydrochloric acid was added to acidify the solution and precipitate boric acid. The boric acid stayed in suspension and was filtered off. The solution was neutralized with 10mL of trimethylamine and 2.59g of triethylammonium chloride dissolved in 50mL of water was added to the solution to substitute the sodium cation with triethylamine. The solution was filtered and the solids were collected.

Revisiting the solution after a couple weeks, the solution was neutralized again with 6mL of trimethylamine. An additional 2.6g triethylammonium chloride was put into the solution before filtering was repeated and more solids were recovered. ^{1}HNMR (D_2O): 1.3 (t, CH_2, 6H), 3.2 (q, CH_3, 9H).

To remove any remaining boric acid, 30mL of water was added, and the suspension was stirred for 2 hours. Then the solids were filtered out and left to dry, they weighed 1.09g, a 24% yield based on moles of iodine.

Substitution of Triethylamine with Cesium

For another cation exchange, 0.92g cesium hydroxide and 10mL of water were added to the solids. These were brought to a boil using a plastic beaker in a water bath. Triethylamine boils at 89°C so only cesium dodecaborohydride remains after recrystallization. This step was repeated with 10mL water. The dry solids weighed 0.92g. ^{11}BNMR (D_2O): -12 (d, $[B_{12}H_{12}]^{2-}$, 12B).

Chapter 5 Boride Results

The main reaction followed Komura et al. [39]and Geis et al. [38] without need for modifications. Since iodine does not readily dissolve in diglyme the solution was constantly stirred up until the addition and the glassware was sized up to much larger than expected for 25g iodine. The reaction of the iodine solution addition to the $NaBH_4$ slurry is immediate and the addition was done drop-by-drop to control the off gassing.

The distillation step is very important to collect all of the solids from the reaction, as the product does not filter easily out of the solution. Secondly maintaining the pH is crucial to separating the boric acid from the dodecaborohydride. When repeating this reaction the collected solids would either be white and crystalline or tan and powdery, as described in Table 8. The tan solids are the dodecaborohydride and the white solids are the boric acid. The solubility of boric acid changes in the aqueous solution and will more readily dissolve when it is acidic. This distinction does not carry over after the cation exchange, as the cesium dodecaborohydride is white and flaky.

The yield was calculated against iodine as it was the limiting reactant, sodium borohydride was used in excess, and it could be directly compare to Geis et al. and Komura et al. Since the yield at 24% is lower than the literature values of 51% for Geis et al. [38] and 53% for Komura et al. [39], care needs to be taken in future experiments for the recovery of product. The yield was calculated by assuming stoichiometric conversion of iodine to sodium iodide, with excess sodium borohydride. Assuming the subsequent reactions were stoichiometric, 15 moles of iodine were needed to make one mole of the dodecaborohydride.

Experiment #	**1**	**2**	**3**
Mass Solids	0.365g	1.09g	0.183g
Description	White crystals	Tan powder	White crystals
^{1}HNMR	No visible peaks	See Figure 41	-

Table 8 Summary of Triethylammonium Dodecaborohydride Results

NMR spectroscopy was used at two different stages of the reaction to verify the presence of the dodecaborohydride and separation from boric acid. Proton spectra at the addition step of triethylammonium chloride showed proton peaks from the hydrogen in the ethyl groups. The only other peak visible is for the residual solvent peak near 4.7ppm. See Figure 41 for the proton NMR.

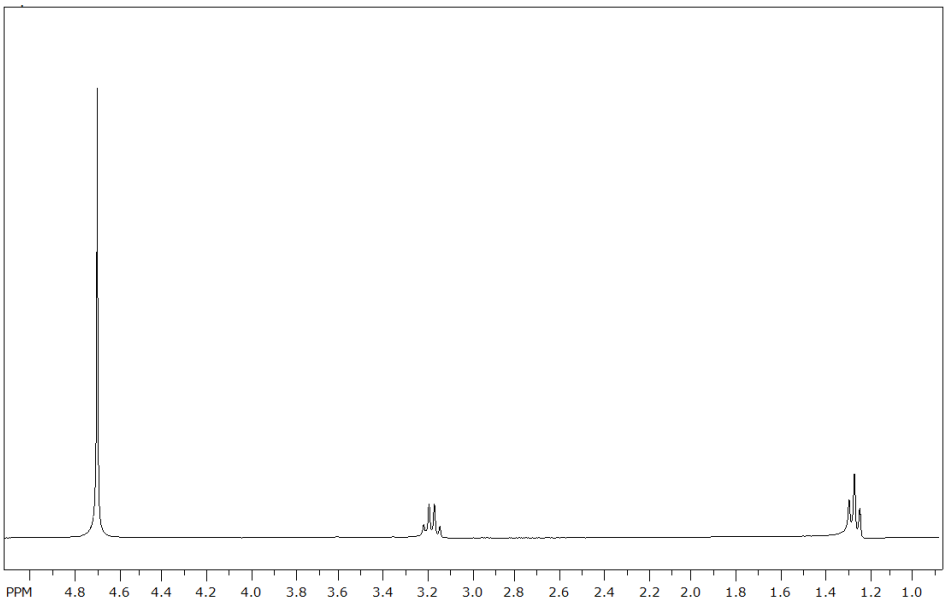

Figure 41 ^{1}HNMR Spectra of $[(C_2H_5)_3N]_2B_{12}H_{12}$

The second sample's spectra were taken after the cation substitution with cesium hydroxide. Since the characteristic boron spectra peaks between dodecaborohydride and boric acid are significantly different, the reaction sample was compared to a known sample of boric acid. For the boron NMR of the product see Figure 42. Boric acid is shown in Figure 43; note the difference in peak placement and division. As borosilicate glass NMR tubes can interfere with boron NMR spectroscopy each of the spectra had a blank of an NMR tube filled with D_2O to the same approximate level as the other two samples, this was subtracted out of the baseline.

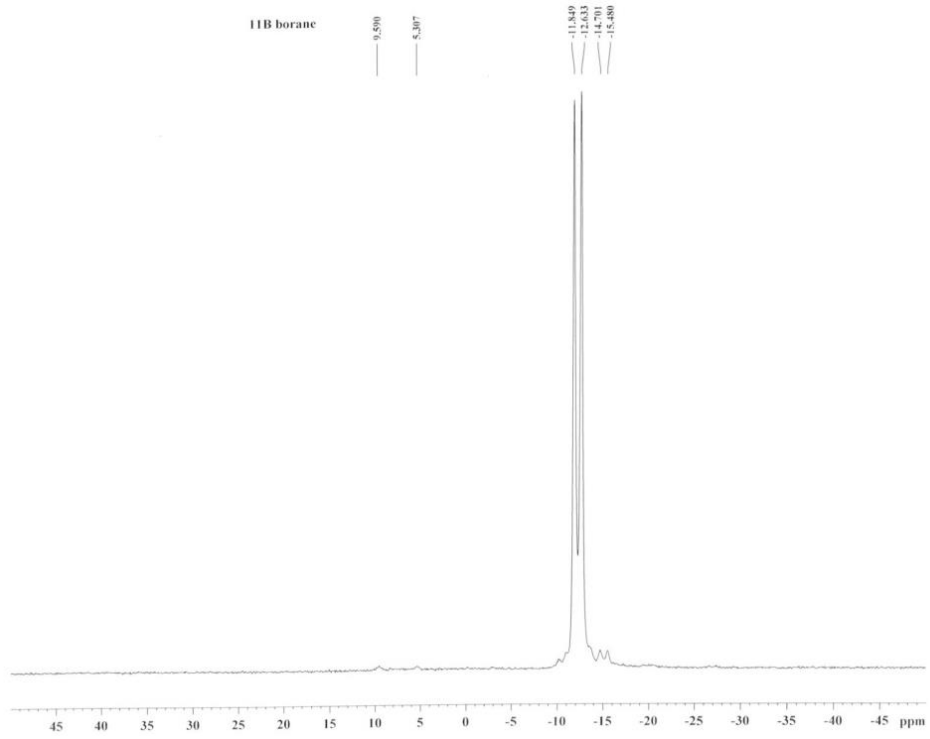

Figure 42 ^{11}BNMR Spectra of $Cs_2B_{12}H_{12}$

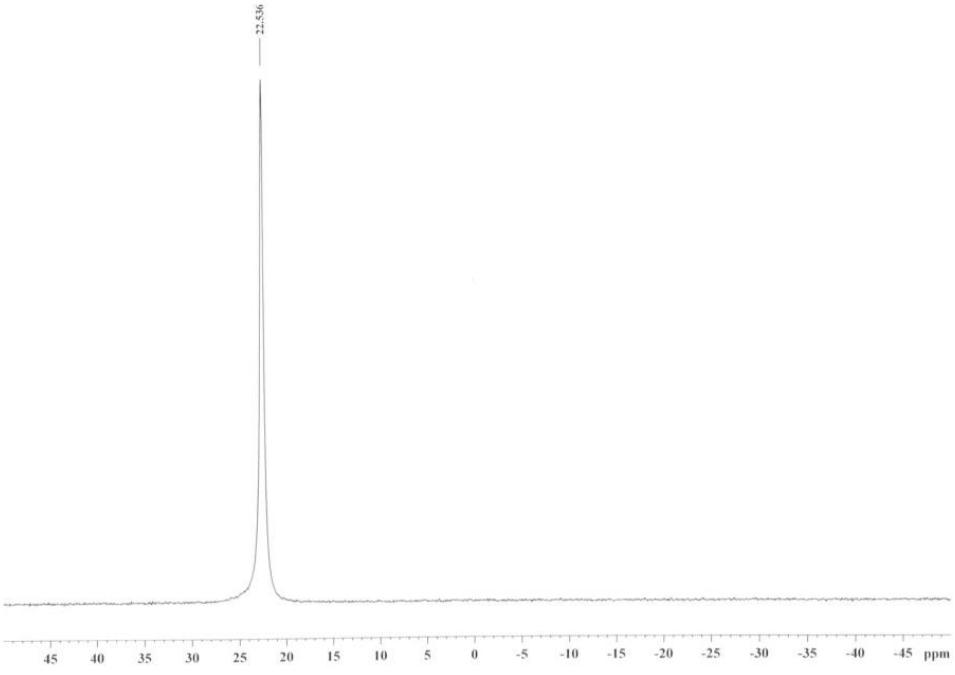

Figure 43 ^{11}BNMR Spectra of Boric Acid

Chapter 6 Conclusion

Among UHTCs, hafnium diboride and carbide are some of the most temperature and oxidation resistant materials. These ceramics can be deposited quicker than traditional methods by pyrolyzing networked polymers. The films could lead to more uniform ceramics that would be beneficial for thermal barrier coatings, used on hypersonic leading edges, replacing less resistant silicon carbide and silicon carbide supported composites.

High surface area active metals like ultrasonically dispersed sodium-potassium alloy and, alternatively, sodium-potassium alloy complexed with 18-crown-6 ether stabilizes the reaction rate of the Wurtz coupling synthesized polycarbynes and reduces the hazards during quenching by using practically all of the reactive metal. However, ultrasonically dispersed sodium-potassium alloy showed NMR peaks with tertiary sp^3 bonded carbon, whereas the crown ether complex formed mostly secondary sp^3 carbon chains. Replacing the solvent with toluene removes a point of oxygen contamination that occurs from ether solvent degradation, though it is chemically bonded in the product; as does working within a dry glove box equipped with regeneration cylinders.

Since the dodecaborohydride synthesis is a more predictable method, there were no significant modifications. It is an effective precursor as it has straightforward initial substitution. Though separating the product from boric acid is very pH sensitive, differentiating between the two through boron NMR is clear. The next step is to incorporate the metal ions in the preceramic dodecaborohydride polymer and to develop a method to form continuous films. Overall there is promise in continuing to develop these synthesis methods as alternatives to current deposition methods for better quality thermal barrier coatings.

Chapter 7 Future Work

Carbide

Further study of the NaK emulsion reaction systems and characterization of the products are recommended to assess if a highly networked sp^3 carbon polymer is being formed. For instance, the possibility of the inclusion of toluene, or other rearrangements, could interfere with the conversion of the polymer to the ceramic. Proton NMR provided by Bianconi et al. is different from the data analyzed in this study in every experimental method, but there are consistent peaks between experimental runs for the toluene solvent based methods.

Additionally, aromatic monosubstituted compounds as reactants following the crown ether method showed that the toluene was included in the dimers that formed. Further study of noninterfering solvents, like benzene, is recommended.

If oxygen-less sp^3 products are being formed from the bromoform coupling, then a method can be developed to incorporate Group 4 metals into the system. From there pyrolysis on the polymer with and without the metal should be attempted and characterization done on the ceramic films produced. Then organometallic precursors can be developed, similar materials to current Group 4 carbide sources for low temperature CVD [1]. From there, further scale up could be studied.

Boride

Dodecaborohydride is straightforward to separate from the boric acid side product and then perform a cation replacement on. Continuing with this method is recommended. The next step is to replace the cesium ions from the dodecaborohydride with titanium, or hafnium. Then verify that the dodecaborohydride can be converted to the diboride via pyrolysis, like the previous work of magnesium borohydride [29] and characterize the ceramic.

Since the current product is a flaky solid or tan powder, development of a coating process would be necessary. In the long term, the scalability of the reaction needs to be explored for the more industrial application.

Works Cited

[1] G. S. Girolami, J. A. Jensen, D. M. Pollina, W. S. Williams, A. E. Kaloyeros and C. M. Allocca, "Organometallic Route to the Chemical Vapor Deposition of Titanium Carbide Films at Exceptionally Low Temperatures," *Journal of the American Chemical Society,* vol. 109, pp. 1579-1580, 1987.

[2] J. M. Criscione, R. A. Mercuri, E. P. Schram, A. W. Smith and H. F. Volk, "High Temperature Protective Coatings for Graphite Part I," Air Force Materials Laboratory Research and Technology Division, Parma, Ohio, 1964.

[3] M. M. Opeka, I. G. Talmy, E. J. Wuchina, J. A. Zaykoski and S. J. Causey, "Mechanical, Thermal, and Oxidation Properties of Refractory Hafnium and Zirconium Compounds," *Journal of the European Ceramic Society,* vol. 19, pp. 2405-2414, 1999.

[4] M. M. Opeka, I. G. Talmy and J. A. Zaykoski, "Oxidation-based materials selection for 2000C+ hypersonic aerosurfaces: Theoretical consideration and historical experience," *Journal of Material Sciences,* vol. 39, pp. 5887-5904, 2004.

[5] W. G. Fahrenholtz, G. E. Hilmas, I. G. Talmy and J. A. Zaykoski, "Refractory Diborides of Zirconium and Hafnium," *Journal of the American Ceramic Society,* vol. 90, pp. 1347-1364, 2007.

[6] S. T. Schwab, C. A. Stewart, K. W. Dudeck, S. M. Kozmina, J. D. Katz, B. Bartram, E. J. Wuchina, W. J. Kroenke and G. Courtin, "Polymeric precursors to refractory metal borides," *Journal of Materials Science,* vol. 39, pp. 6051-6055, 2004.

[7] T. H. Squire and J. Marschall, "Material Property Requirements For Analysis and Design of UHTC Components in Hypersonic Applications," *Journal of the European Ceramic Society,* vol. 30, pp. 2239-2251, 2010.

[8] W. A. Frad, "Metal Carbides," in *Advances in Inorganic Chemistry and Radiochemistry, Vol. 11*, New York, Academic Press, 1968, pp. 153-238.

[9] E. Wuchina, M. Opeka, S. Causey, K. Buesking, J. Spain, A. Cull, J. Routbort and F. Guitierrez-Mora, "Designing for Ultrahigh-Temperature Applications:The Mechanical and Thermal Properties of HfB2, HfCx, HfNx, and alphaHf(N)," *Journal of Materials Science,* vol. 39, pp. 5939-5949, 2004.

[10] A. Paul, J. Binner and B. Vaidhyanathan, "UHTC Composites for Hypersonic Applications," in *Ultra-High Temperature Ceramics: Materials for Extreme Environment Applications*, Hoboken, John Wiley & Sons, Inc., 2014, pp. 144-166.

[11] P. A. Bianconi, S. J. Joray, B. L. Aldrich, J. Sumranjit, D. J. Duffy, D. P. Long, J. L. Lazorcik, L. Raboin, J. K. Kearns, S. L. Smulligan and J. M. Babyak, "Diamond and Diamond-Like Carbon from a Preceramic Polymer," *Journal of the American Chemical Society,* vol. 126, pp. 3191-3202, 2004.

[12] R. J. Corriu, "Ceramics and Nanostructures from Molecular Precursors," *Angewandte Chemie,* vol. 39, pp. 1376-1398, 2000.

[13] B. Boury, R. J. Corriu, D. Leclerco, H. Mutin, J. M. Planeix and A. Vioux, "A Catalytic Preparation of a New Preceramic Polymer: Transformation Into SiC," in *Inorganic and Organometallic Polymers with Special Properties*, Boston, Kluwer Academic Publishers, 1992, pp. 255-266.

[14] I. D. Miller, D. Thompson, R. Sooriyakumaran and G. N. Fickes, "The Synthesis of Soluble, Substituted Silane High Polymers by Wurtz Coupling Techniques," *Journal of Polymer Science Part A: Polymer Chemistry,* vol. 29, pp. 813-824, 1991.

[15] J. A. Jensen, J. E. Gozum, D. M. Pollina and G. S. Girolami, "Titanium, Zirconium, and Hafnium Tetrahydroborates as "Tailored" CVD Precursors for Metal Diboride Thin Film," *Journal of the American Chemical Society,* vol. 110, pp. 1643-1644, 1988.

[16] J. M. Criscione, H. F. Volk, J. W. Nuss, R. A. Mercuri, S. Sarian and F. W. Meszaros, "High Temperature Protective Coatings for Graphite Part III," Air Force Materials Laboratory Metals and Ceramics Division, Parma, 1965.

[17] J. M. Criscione, S. Sarian, H. F. Volk, J. W. Nuss and F. W. Meszaros, "High Temperature Protective Coatings for Graphite Part IV," Air Force Materials Laboratory Research and Technology Division, Parma, 1966.

[18] R. Ruh and V. A. Patel, "Proposed Phase Relations in the HfO2-Rich Portion of the System Hf-HfO2," *Journal of the American Ceramic Society,* vol. 56, pp. 606-607, 1973.

[19] Y. Wang, X. Xiong, G. Li, H. Zhang, Z. Chen, W. Zun and X. Zhao, "Microstructure and Ablation Behavior of Hafnium Carbide Coating for Carbon/Carbon Composites," *Surface & Coatings Technology,* vol. 206, pp. 2825-2832, 2012.

[20] C. Frondel and U. B. Marvin, "Lonsdaleite, a Hexagonal Polymorph of Diamond," *Nature,* vol. 214, pp. 587-589, 1967.

[21] Y. Nur, M. W. Pitcher, S. Settudoglu and L. Toppare, "Facile Synthesis of Poly(hydridocarbyne): A Precursor to Diamond and Diamond-Like Ceramics," *Journal of Macromolecular Science, Part A: Pure and Applied Chemistry,* vol. 45, pp. 358-363, 2008.

[22] M. Mostoller, T. Kaplan and M. Chisholm, "Edge Dislocations in Silicon," [Online]. Available: http://web.ornl.gov/info/ornlreview/v30n3-4/edge.htm. [Accessed 5 May 2014].

[23] M. Schmidt, "Qucosa," 12 March 2012. [Online]. Available: http://www.qucosa.de/recherche/frontdoor/?tx_slubopus4frontend[id]=8448. [Accessed 5 May 2014].

[24] Q. Zeng, J. Peng, A. R. Oganov, Q. Zhu, C. Xie, X. Zhang, D. Dong, L. Zhang and L. Cheng, "Prediction of Stable Hafnium Carbides: Stoichiometries, Mechanical Properties, and Electronic Structure," *Physical Review B,* vol. 88, pp. 214107(1)-214107(6), 2013.

[25] H. Fujii and K. Ozawa, "Critical temperature and carbon substitution in MgB2 prepared through the decomposition of Mg(BH4)2," *Superconducting Science and Technology,* vol. 23, pp. 125012-125017, 2010.

[26] D. L. Segal, "Chemical Routes for the Preparation of Powders," in *The Physics and Chemistry of Carbides, Nitrides and Borides*, New York, Kluwer Academic Publishers, 1990, pp. 3-11.

[27] H. R. Hoekstra and J. J. Katz, "The Preparation and Properties of the Group IV-B Metal Borohydrides," *Journal of the American Chemical Society,* vol. 71, pp. 2488-2492, 1949.

[28] A. L. Wayda, L. F. Schneemeyer and R. L. Opila, "Low-Temperature Deposition of Zirconium and Hafnium Boride Films by Thermal Decomposition of the Metal Borohydrides (M[BH4]4)," *Applied Physics Letters,* vol. 53, pp. 361-363, 1988.

[29] S. Gupta, I. Z. Hlova, T. Kobayashi, R. V. Denys, F. Chen, I. Y. Zavaliy, M. Pruski and V. K. Pecharsky, "Facile synthesis and regeneration of Mg(BH4)2 by high energy reactive ball milling of MgB2," *Chemical Communication,* vol. 49, pp. 828-830, 2013.

[30] D. M. Goedde and G. S. Girolami, "A New Class of CVD Precursors to Metal Borides: Cr(B3H8)2 and Related Octahydrotriborate Complexes," *Journal of the American Chemical Society,* vol. 126, pp. 12230-12231, 2004.

[31] T. D. Lash and D. Berry, "Promotion of Organic Reactions by Ultrasound: Coupling of Alkyl and Aryl Halides in the Presence of Lithium Metal and Ultrasound," *Journal of Chemical Education,* vol. 62, p. 85, 1985.

[32] D. VanderBurg and G. J. Price, "Ultrasound promoted Wurtz coupling of alkyl bromides and dibromides," *Ultrasonics Sonochemistry,* vol. 19, pp. 5-8, 2012.

[33] G. T. Visscher and P. A. Bianconi, "Synthesis and Characterizatoin of Polycarbynes, a New Class of Carbon-Based Network Polymers," *Journal of American Chemical Society,* vol. 116, pp. 1805-1811, 1994.

[34] L. Mesazaros, "Pyrophoric Lead as a New Agent of Wurtz-Like Reactions," *Tetrahedron Letters,* vol. 49, pp. 4951-4952, 1967.

[35] M. W. Pratt, R. Helsby and H. M. Stanier, "Ultrasonically Dispersed Sodium," *Nature,* vol. 184, pp. 284-289, 1959.

[36] C. Einhorn, J. Einhorn and J.-L. Luche, "Sonochemistry-The Use of Ultrasonic Waves in Synthetic Organic Chemistry," *Synthesis,* vol. 11, pp. 787-813, 1989.

[37] D. Segal, Chemical Synthesis of Advanced Ceramic Materials, Cambridge: Cambridge University Press, 1989.

[38] V. Geis, K. Guttsche, C. Knapp, H. Scherer and R. Uzun, "Synthesis and characterization of synthetically useful salts of the weakly-coordinating dianion [B12Cl12]2-," *Dalton Transactions,* no. 15, pp. 2687-2694, 2009.

[39] M. Komura, K. Aono, K. Nagasawa and S. Sumimoto, "A Convenient Preparation of 10B-Enriched B12H12SH2- an Agent for Neutron Capture Therapy," *Chemistry Express,* vol. 2, pp. 173-176, 1987.

[40] Sigma-Aldrich, "Technical Information Bulletin A-143," Aldrich, 2013. [Online]. Available: http://www.sigmaaldrich.com/chemistry/chemical-synthesis/learning-center/technical-bulletins/al-1430.html. [Accessed July 2014].

[41] Y. Nur, S. Dygulu, M. W. Pitcher and L. Toppare, "The Electrochemical Synthesis of Poly(methylcarbyne) for Diamond Film Coatings," *Journal of Applied Polymer Science,* vol. 124, pp. 3626-3632, 2011.

[42] Kemika, "Material Safety Data Sheet SiGNa Na-Silica Gel (Stage I)," SiGNa Chemistry, Inc, New York, 2007.

[43] A. I. Sizov, T. M. Zvukova and B. M. Bulychev, "Mechanochemical Synthesis of Poly(hydridocarbyne)," *Russian Chemical Bulletin, International Edition,* vol. 61, pp. 668-669, 2012.

[44] M. D. Koretsky, Engineering and Chemical Thermodynamics, Hoboken: John Wiley & Sons, Inc., 2004.

[45] J. L. Dye, K. D. Cram, S. A. Urbin, M. Y. Redko, J. E. Jackson and M. Lefenfeld, "Alkali Metals Plus Silica Gel: Powerful Reducing Agents and Convenient Hydrogen Sources," *Journal of the American Chemical Society Communications,* vol. 127, pp. 9338-9339, 2005.

[46] G. R. Fulmer, A. J. Miller, N. H. Sherden, H. E. Gottlieb, A. Nudelman, B. M. Stoltz, J. E. Bercaw and K. I. Goldberg, "NMR Chemical Shifts of Trace Impurities: Common Laboratory Solvents, Organics, and Gases in Deuterated," *Organometallics,* vol. 29, pp. 2176-2179, 2010.

[47] B. J. Filla and J. E. Callanan, "Laboratory-Scale Controlled-Atmosphere Chamber for Use with Premium Coal Samples," *Review of Scientific Instruments,* vol. 56, pp. 592-595, 1985.

[48] H. J. Gardner, "An Improved Glove Box with High Purity Atmosphere," *Journal of Physics E: Scientific Instruments,* vol. 3, pp. 569-570, 1970.

[49] D. J. Artrip, "Reduction Guidelines for Copper Catalysts," Research Catalysts, Inc., Houston, 2012.

[50] G. Bojase, T. V. Nguyen, A. D. Payne, A. C. Willis and M. S. Sherburn, "Synthesis and Properties of the Ivyvanes: the Parent 1,1-oligocyclopropanes," *Chemical Science,* vol. 2, pp. 229-232, 2011.

[51] J. J. Eisch, "Chemistry of Alkali Metal-Unsaturated Hydrocarbon Adducts III. Cleavage Reactions by Lithium-Biphenyl Solutions in Tetrahydrofuran," *Journal of Organic Chemistry,* vol. 28, pp. 707-710, 1963.

[52] C. J. Pedersen, "Cyclic Polyethers and Their Complexes with Metal Salts," *Journal of the American Chemical Society,* vol. 89, pp. 7017-7036, 1967.

[53] T. Yamaji, T. Saito, T. Hayamizu, M. Yanagisawa, O. Yamamoto, N. Wasada, K. Someno, K. Kinugasa, K. Tanabe, T. Tamura and J. Hiraishi, "Spectral Database for Organic Compounds SDBS," National Institute of Advanced Industrial Science and Technology, 4 April 2012. [Online]. Available: http://sdbs.db.aist.go.jp/sdbs/cgi-bin/cre_index.cgi. [Accessed 21 April 2015].

[54] P. J. Linstrom, "NIST Chemistry WebBook," National Institute of Standards and Technology, 2011. [Online]. Available: http://webbook.nist.gov/chemistry/. [Accessed 11 May 2015].

[55] A. Mikaia, E. White, V. Zaikin, D. Zhu, B. Milman, V. Babushok, I. Zenkevich, P. Linstron, Y. Mirokhin, D. Tchekhovskoi, W. G. Mallard, O. D. Sparkman and J. A. Sparkman, "NIST/EPA/NIH Mass Spectral Library (NIST 08) and NIST Mass Spectral Search Program (Version 2.0f)," U.S. Department of Commerce, Gaithersburg, 2008.

Appendices

Appendix A Glove Box Diagrams and Operating Procedures

Glove Box Flow Diagram

As a reference to the photos in Chapter 3, Figure 44 shows the flow layout of the glove box.

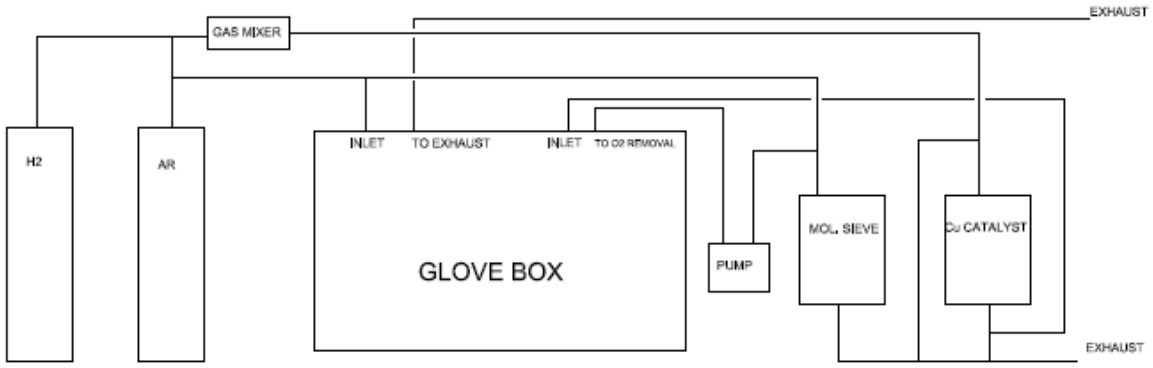

Figure 44 Glove Box Flow Diagram

Proposed Gas Mixer Piping and Instrumentation Diagram

The piping and instrumentation diagram (P&ID) shown in Figure 45 was proposed for copper catalyst regeneration to avoid purchasing expensive pre-mixed hydrogen-argon gas. Before this piping layout could be implemented, the gas mixer was purchased and installed.

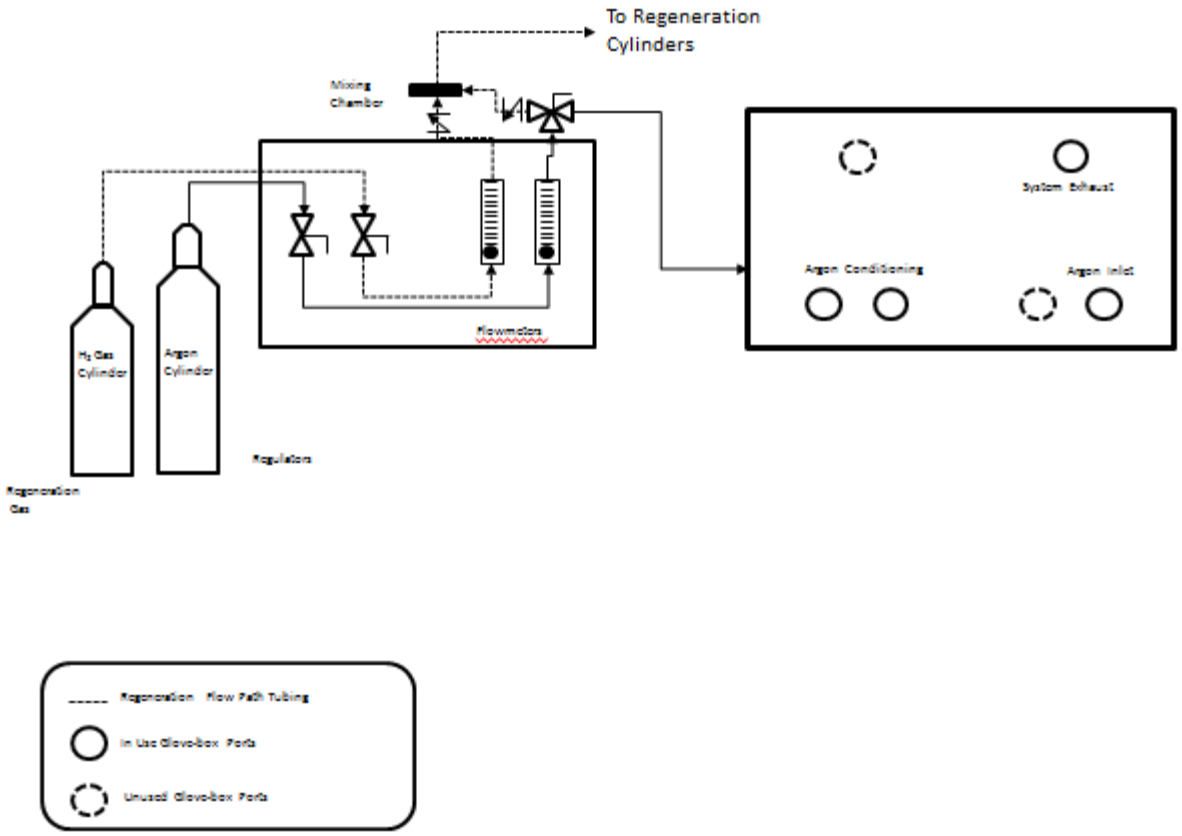

Figure 45 Proposed Gas Mixer P&ID

Standard Operating Procedure for Transferring Items in and out of the Glove Box

Step 1: Put items from the outside into the glove box transfer chamber, making sure the door is secured. Turn on the Ar and let a trickle of Ar into the glove box, this will keep the pressure positive in the glove box.

Step 2: Open the valve from the transfer chamber to the vacuum pump. Turn on the pump and let it run until the meter reads approximately -15 inHg. Turn off the pump and close the valve to it.

Step 3: Open the valve between the glove box and the transfer chamber gradually. Once the pressure of the transfer chamber is equal to the glove box, close the valve between them.

NOTE: Do not pump down the transfer chamber when it is open to the glove box, as it could create negative pressure in the glove box.

Step 4: Repeat Step 2 and Step 3 one more time to reduce the amount of oxygen in the transfer chamber.

Step 5: Turn off the Ar and close the inlet valve from the Ar to the glove box. Open the inner transfer chamber door to take out the items. Close the transfer chamber door.

Step 6: To put items in from the glove box to the transfer chamber in this state there is no need for another purge. To take the items back outside, open the outer transfer chamber door, however, now to move more items out of the glove box a purge would be needed.

NOTE: It is better to assume the transfer chamber is filled with ambient air rather than the glove box atmosphere. When in doubt purge the transfer chamber twice before opening it to the glove box.

Standard Operating Procedure for Copper Catalyst Regeneration

Discrepancies from this section and the procedure listed in Chapter 2 are due to the observance of heat zones in the cylinder that reached above the recommended operating conditions.

Step 1: Make sure that the Ar feed valve to the catalyst cylinder is open, as well as the three way valve for exhaust from the catalyst cylinder. If not already purged with Ar, start 5 SLPM of Ar per 5 kg catalyst for 2hrs. Set up a precipitation-trap on the end of the exhaust to collect water driven off from the catalyst. See Figure 46.

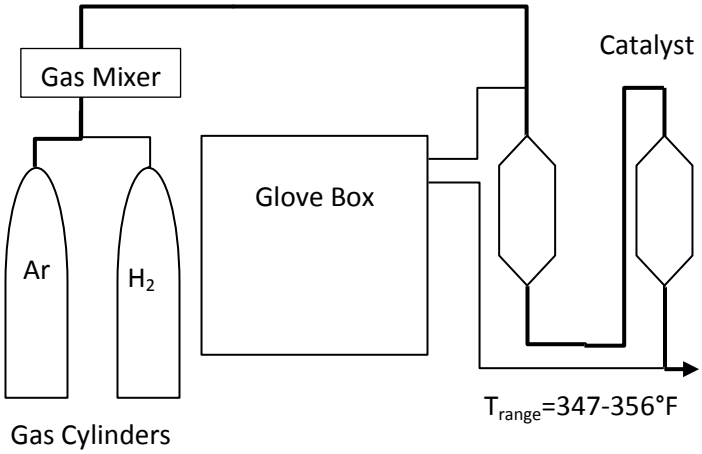

Figure 46 Cu Catalyst Cylinder Purge

Step 2: Adjust flow to 5-25 SLPM and adjust gas mixer to 1.33% H_2/Ar mixture per kg catalyst, increase temperature on the controller to 325°F. At 5 SLPM it takes 24 hrs for the catalyst to reduce, at 15 SLPM it takes 5 hrs. This takes several Ar cylinders. The regeneration is complete when the catalyst temperature drops following the “hot zone” passing through the system. DO NOT adjust the H_2 gas percentage above the lower flammability limit. See Figure 47.

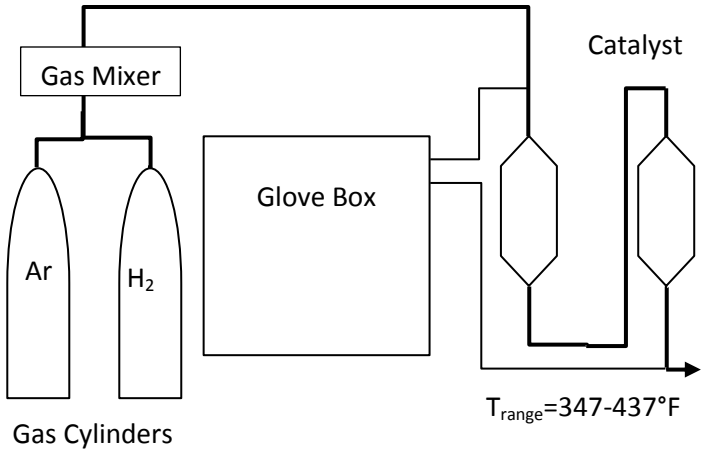

Figure 47 Cu Catalyst Cylinder Regeneration

Step 3: Purge with Ar for 1 hr. Turn off temperature controller and let return to ambient temperatures. Then turn off Ar and its feed valve to the catalyst cylinder. Turn the three-way exhaust valve so that it runs back to the glove box and the three-way inlet valve to the catalyst cylinder so that it flows from the glove box. See Figure 48.

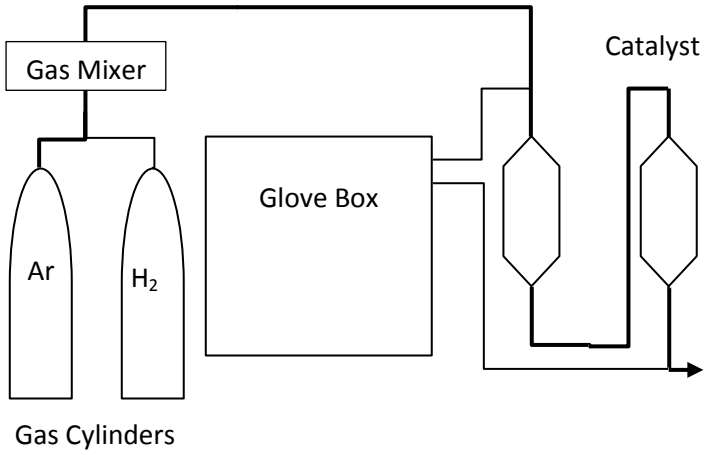

Figure 48 Cu Catalyst Cylinder Cooling Purge

Step 4: To remove water vapor and oxygen from the glove box, adjust temperature controller to 300°F and turn on recirculation pump. See Figure 49.

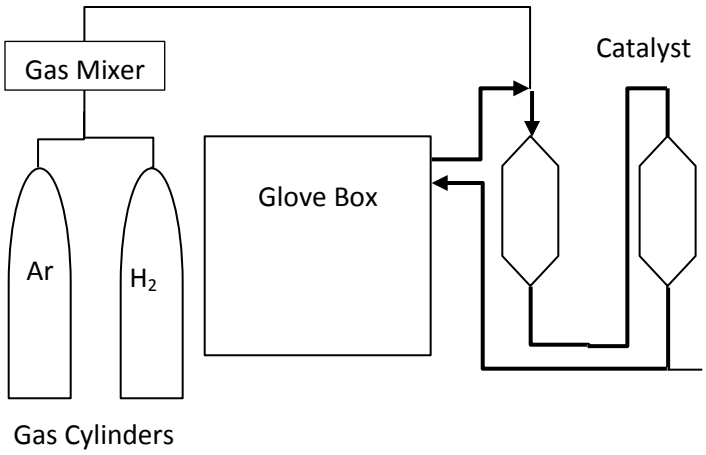

Figure 49 Recirculation of Glove Box Atmosphere

Appendix B Experimental Equipment

Thermoelectric Cooling Block

Figure 50 shows the pentagonal design of the cooling block. Though it is specified as copper, aluminum was found to be more cost effective and still was effective at removing heat from the reaction vessel. The inner radius is 4.5cm. The cooling units were attached with long screws and the contact between the Peltier face and the aluminum was coated in thermal paste.

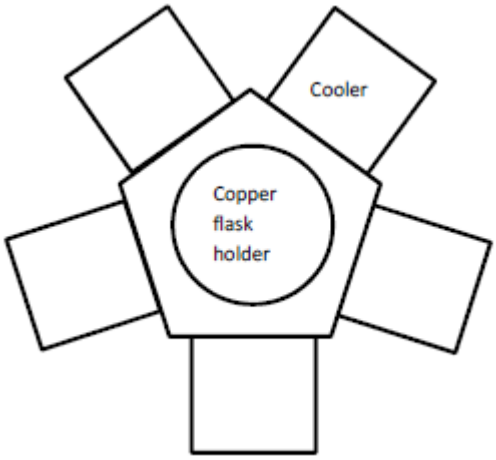

Figure 50 Cooling Block Design Schematic

Ultrasonic Probe Energy and Power Tables

The controller on the ultrasonic probe has energy, in Joules, and power output, in Watts (J/s), readings. As the energy output was an incremental reading, as opposed to the instantaneous power measurement, it was easier to evaluate.

In Table 9, Table 10, and Table 11 the energy provided by the ultrasonic probe immersed in a beaker of water over time at specific amplitudes was recorded and then the average power was calculated in Table 12. These measurements were made without the pulse and the extrapolated data points are highlighted. Breaks in the table and inconsistencies in time are from when sonication caused the water to boil, throwing off the energy measurements. Due to the autotuning feature of the probe, there is about 30s where the energy output is not stable after a change in amplitude.

Time (s)	Amp (%)	Energy (J)
105	20	850
140	30	1133.3
190	30	1970
240	35	2806.7
290	35	3740
330	40	4486.7
375	40	5530
450	45	7268.9
510	45	8850

Table 9 Energy Output from 20% to 45% Amplitude

Time (s)	Amp (%)	Energy (J)
30	45	670
100	45	2800
150	45	3900
200	50	5185.0
240	50	6570

Table 10 Energy Output from 45% to 50% Amplitude

Time (s)	Amp (%)	Energy (J)
30	50	770
70	50	2090
120	50	3670
180	50	5470
210	55	6343.0
230	55	7000
290	55	9190
330	55	10440
350	60	11097
380	60	12180
430	60	14000
480	60	15990
530	60	17900
600	65	20526.8
630	65	21780
690	65	23990
750	65	26250

795	70	27994.2
815	70	28890
860	70	30750
920	70	33150

Table 11 Energy Output from 50% to 70% Amplitude

Amp (%)	Power (J/s)
20	8.1
30	16.7
35	18.7
40	23.2
45	25.7
50	29.1
55	32.9
60	37.5
65	38.8
70	42.0

Table 12 Power Calculated

Appendix C GC-MS Data Tables

Bromobenzene, in Table 13, and 2-bromotoluene samples, in Table 14, were diluted with methylene chloride for analysis. The chemical compounds were confirmed by mass spectral matching with the National Institute of Standards and Technology (NIST) 2008 Library, only the top matches were included in the table [55].

Bromobenzene Product Peak List				
Apex RT (min)	**%Area**	**%Height**	**%Match** [55]	**Compound** [55]
3.79	0.04	0.08		
7.42	6.67	9.53	94.95%	Bromobenzene
18.65	0.83	0.46		
19.9	9.96	11.22	51.19%	Biphenyl
20.04	0.8	0.82		
20.51	8.22	8.87	20.21%	2-Methyl Biphenyl
20.72	0.12	0.13		
20.81	0.04	0.06		
20.87	0.04	0.06		
21.01	0.03	0.05		
21.23	19.17	21.51	23.80%	4-Methyl Biphenyl
21.46	0.21	0.26		
21.64	0.13	0.17		
22.04	0.05	0.07		
22.59	1.96	2.25	27.30%	4-Methyl Biphenyl
22.79	6.98	8.01	30.40%	4-Methyl Biphenyl
23.41	5.16	5.57	86.50%	Bibenzyl
23.72	0.21	0.23		
23.86	0.04	0.05		
24.11	0.02	0.04		
24.61	0.03	0.03		
25.13	0.36	0.38		
25.29	0.11	0.09		
25.64	0.06	0.06		
25.86	0.03	0.03		
26.36	0.1	0.13		
26.49	0.25	0.18		
27.14	0.09	0.11		
27.27	0.26	0.32		
27.38	6.07	7	68.52%	3-Bromo Diphenylmethane

27.63	0.04	0.04		
29.42	0.05	0.05		
29.73	0.03	0.04		
29.8	0.03	0.04		
29.9	0.02	0.02		
29.92	0.05	0.02		
30.09	0.03	0.02		
31.03	0.17	0.19		
31.31	1.44	1.75		
31.94	0.25	0.31		
32.61	1.92	0.53		
33.15	0.18	0.2		
33.36	0.07	0.08		
33.51	4.74	4.91	37.92%	Triphenylmethane
33.62	2.3	2.43	40.92%	2-Benzyl Biphenyl
34.16	0.05	0.05		
34.3	0.11	0.09		
34.78	0.22	0.18		
35.05	0.07	0.03		
35.31	0.17	0.15		
35.78	0.53	0.44		
35.96	0.43	0.2		
36.56	0.07	0.04		
36.98	0.17	0.1		
37.27	0.65	0.32		
37.67	0.95	0.59		
38.16	2.3	1.39		
39.56	3.99	2.26	29.33%	4-Benzyl Biphenyl
39.71	8.3	4.56		
39.96	2.19	1.02		
40.6	0.2	0.07		
41.4	0.19	0.09		

Table 13 GC-MS Bromobenzene Product Peak List

2-Bromotoluene Product Peak List				
Apex RT (min)	**%Area**	**%Height**	**%Match** [55]	**Compound** [55]
3.78	0.99	1.7		
10.51	63.76	64.81	31.50%	m-Bromotoluene
21.2	2.11	2.4		
22.66	0.03	0.04		

22.88	0.47	0.53		
23.19	2.73	3.01	21.90%	2,2'-Dimethyl biphenyl
23.41	4.36	4.58	89.50%	Bibenzyl
23.57	1.12	1.3		
23.64	10.57	11.8	28.00%	1-Methyl-4-(phenylmethyl)benzene
23.86	0.07	0.07		
25.34	0.15	0.16		
26.86	0.04	0.05		
27.14	0.06	0.06		
27.26	0.56	0.58		
27.41	0.04	0.05		
27.5	0.44	0.42		
27.74	0.05	0.06		
28.83	0.08	0.09		
29.31	0.9	0.44		
29.7	0.07	0.08		
29.8	0.1	0.11		
31.03	0.61	0.65		
31.51	0.03	0.04		
33.13	0.1	0.1		
34.44	0.17	0.17		
35.24	0.65	0.54		
36	4.07	2.97	80.72%	7,7-Dimethyl-2,4-diphenyl-1,3,5-cycloheptatriene
36.56	1.02	0.75		
36.8	0.36	0.27		
36.94	0.13	0.07		
37.67	0.7	0.43		
37.95	1.55	0.77		
38.84	0.06	0.04		
39	0.07	0.05		
40.65	0.08	0.04		
40.9	0.23	0.13		
41.23	0.5	0.19		
42.12	0.04	0.03		
42.51	0.85	0.38		
42.89	0.09	0.04		

Table 14 GC-MS 2-Bromotoluene Product Peak List